A Numerical Study of Flow of Newtonian and Non-Newtonian Fluids Past a Square Cylinder in a Rectangular Channel

By

Mukesh Gupta

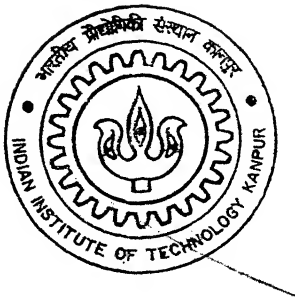

DEPARTMENT OF MECHANICAL ENGINEERING

Indian Institute of Technology Kanpur

FEBRUARY, 2003

A Numerical Study of Flow of Newtonian and Non-Newtonian Fluids Past a Square Cylinder in a Rectangular Channel

A thesis submitted

in partial fulfilment of the requirements

for the degree of

Master of Technology

by

Mukesh Gupta

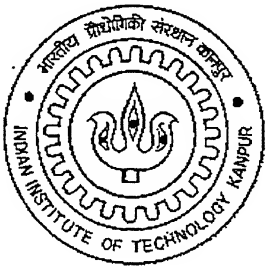

to the

Department of Mechanical Engineering

Indian Institute of Technology Kanpur - 208016.

February, 2003

CERTIFICATE

It is certified that the work contained in the thesis entitled **A Numerical Study of Flow of Newtonian and Non-Newtonian Fluids Past a Square Cylinder in a Rectangular Channel** by **Mukesh Gupta (Roll No. Y110518)** has been carried out under our supervision and this work has not been submitted elsewhere for a degree.

Dr.P.S.Ghoshdastidar
Professor
Department of Mechanical Engineering
Indian Institute of Technology Kanpur
Kanpur, U.P.208016

Dr.R.P.Chhabra
Professor
Department of Chemical Engineering
Indian Institute of Technology Kanpur
Kanpur, U.P.208016

February, 2003

Kanpur

Acknowledgement

I would like to express my sincere gratitude, regards and thanks to my thesis supervisors Dr. P.S.Ghoshdastidar and Dr. R.P. Chhabra for their invaluable guidance, suggestions and generous help at all the stages of my research work. They have helped me not only in introducing the exciting field of research, but also in the successful completion of the thesis through their cooperation and encouragement. Their interest and confidence in me was the reason for all the success I have made.

I am extremely grateful to my friends Abhay, Abhishek, Arvind, Atanu, Debadi, Anil and Arun for all the encouragement and support I received from them at all times. It's the combined effort of my friends that the life at I.I.T. Kanpur became enjoyable and memorable.

Mukesh Gupta

Abstract

The incompressible and steady flow of fluid over a square cylinder represents an idealization of many industrially important processes, e.g. chimneys, tubular heat exchangers, towers, flow dividers in polymer processing applications etc. A wealth of information is available on their drag and heat transfer characteristics when the liquid phase exhibits the standard Newtonian fluid behaviour. In contrast, virtually no analogous results are available even for the simplest type of Non-Newtonian fluid behaviour, namely, shear- thinning and shear thickening fluids modeled by the usual two-parameter power law model.

The confined flow of power law fluid past a cylinder with square cross-section mounted in a rectangular channel has been investigated. The present study is concerned with steady flow at low Reynolds numbers. In order to restrict the problem to steady flow, the largest Reynolds number chosen was $\mathrm{Re} = 50.0$ based on maximum velocity at inlet and the chord length of the square cylinder. Two-dimensional computational study has been reported. In the present study for the Non-Newtonian fluid, power law model has been used. The power law fluid is characterized by two parameters, flow consistency index and power law index.

The Stream function-Vorticity approach has been employed to solve the unsteady Navier-Stocks equations through false transient method. Velocity profile and different parameters such as drag coefficient, recirculation length have been computed. The effect of power law index (shear thickening effect, $1.0 \le n \le 1.6$) and blockage ratio ($B = 1/8, 1/6, 1/4$) has been investigated. Grid independence study also has been studied.

Contents

List of figures

Page No

List of tables

Nomenclature

LX	Length of the channel[1]
LY	Width of the channel[1]
L_a	Upstream length of the channel[1]
D	Obstacle width
C_D	Drag coefficient (Equation 2.17)
C_{D_f}	Viscous drag coefficient (Equation 2.18)
C_{D_p}	Form drag coefficient (Equation 2.19)
U	Stream wise component of velocity[1]
V	Transverse component of velocity[1]
ω	Vorticity[1]
ψ	Stream function[1]
P	Pressure[1]
n	Power law index
m	Flow consistency index
Re	Reynolds number (Equation 2.13)
η	Non-newtonian viscosity of fluid, N.Sec/m^2 (Equation 2.9)
μ	Dynamic (newtonian) viscosity of fluid, N.Sec/m^2
ρ	Density, kg/m^3
τ	Stress tensor[1]
X,Y	Stream wise and transverse coordinates[1]

[1]: All variables are nondimensionalized

Chapter 1

INTRODUCTION

1.1 Introduction:

The incompressible and steady flow of fluids around bluff bodies represents an idealization of many industrially important processes, e.g. chimneys, tubular heat exchangers, offshore structures and pipelines, suspension bridges, towers, masts, wires and flow dividers in polymer processing applications etc. The flow past bluff bodies, especially cylinders, has been an attraction in all kinds of fluid mechanical investigations for a long time. Most of these studies were concerned with the circular cylinder case .In recent years; the attention to flow around rectangular cylinders has accelerated, albeit only for Newtonian liquids. A wealth of information is available on drag and heat transfer characteristics when the liquid phase exhibits the standard Newtonian behaviour. In contrast, virtually no corresponding results are available even for the simplest type of Non-Newtonian behaviour, namely, shear-thinning and shear-thickening modeled by the usual two parameter, power law model fluid.

1.2 Literature review:

The literature pertaining to flow past a square cylinder is reviewed below. All literatures are concerned with the behaviour of Newtonian fluid. A review of the earlier investigations related to the different aspects of the flow over low Reynolds numbers has been presented. Viscous flow of Newtonian fluid has

Chapter 1

INTRODUCTION

1.1 Introduction:

The incompressible and steady flow of fluids around bluff bodies represents an idealization of many industrially important processes, e.g. chimneys, tubular heat exchangers, offshore structures and pipelines, suspension bridges, towers, masts, wires and flow dividers in polymer processing applications etc. The flow past bluff bodies, especially cylinders, has been an attraction in all kinds of fluid mechanical investigations for a long time. Most of these studies were concerned with the circular cylinder case .In recent years; the attention to flow around rectangular cylinders has accelerated, albeit only for Newtonian liquids. A wealth of information is available on drag and heat transfer characteristics when the liquid phase exhibits the standard Newtonian behaviour. In contrast, virtually no corresponding results are available even for the simplest type of Non-Newtonian behaviour, namely, shear-thinning and shear-thickening modeled by the usual two parameter, power law model fluid.

1.2 Literature review:

The literature pertaining to flow past a square cylinder is reviewed below. All literatures are concerned with the behaviour of Newtonian fluid. A review of the earlier investigations related to the different aspects of the flow over low Reynolds numbers has been presented. Viscous flow of Newtonian fluid has

Chapter 1

INTRODUCTION

1.1 Introduction:

The incompressible and steady flow of fluids around bluff bodies represents an idealization of many industrially important processes, e.g. chimneys, tubular heat exchangers, offshore structures and pipelines, suspension bridges, towers, masts, wires and flow dividers in polymer processing applications etc. The flow past bluff bodies, especially cylinders, has been an attraction in all kinds of fluid mechanical investigations for a long time. Most of these studies were concerned with the circular cylinder case .In recent years; the attention to flow around rectangular cylinders has accelerated, albeit only for Newtonian liquids. A wealth of information is available on drag and heat transfer characteristics when the liquid phase exhibits the standard Newtonian behaviour. In contrast, virtually no corresponding results are available even for the simplest type of Non-Newtonian behaviour, namely, shear-thinning and shear-thickening modeled by the usual two parameter, power law model fluid.

1.2 Literature review:

The literature pertaining to flow past a square cylinder is reviewed below. All literatures are concerned with the behaviour of Newtonian fluid. A review of the earlier investigations related to the different aspects of the flow over low Reynolds numbers has been presented. Viscous flow of Newtonian fluid has

been studied extensively in the past. Thus for instance, at low to moderate Reynolds numbers, such flows have been computed by Davis and Moore (1982), Okajima (1982), Davis et al. (1984), Franke et al. (1990), Okajima et al. (1990), Kelkar and Patankar (1992), Mukhopadhyay et al. (1992), Zaki et al. (1994), Sohankar et al. (1995), Valencia (1995), Saha et al. (2000), Breuer et al. (2000) etc.

Flow of Newtonian fluid past a square cylinder shows the following behaviour with increasing Reynolds number. In the Reynolds number range of 2-8, the flow is unseparated and symmetric above & below the cylinder with respect to the axis aligned with the flow. Once the Reynolds number exceeds certain limit, separation at the leading edge is observed. This is followed by reattachment over the sides of the cylinder and separation once again at the trailing edge and a closed steady recirculation region consisting of two symmetric vortices is observed behind the cylinder. The size of recirculation region increases with increase in Reynolds number. When a certain threshold limit is crossed the vortex shedding can be detected in the wake showing the unsteadiness in the flow behind the cylinder, this Reynolds number is called critical Reynolds number.

Many researchers have found different value of critical Reynolds number experimentally and numerically. Based on experiment investigations, Okajima (1982) found the periodic vortex motion to occur at Reynolds number$\approx$70 thus leading to an upper limit of critical Reynolds number $\leq$70. A smaller value (Re=54) was determined by Kelkar and Patankar (1992) based on the stability analysis of the flow. According the numerical study done by Mukhopadhyaya (1992), the wake losses its original symmetry at Re=85 and flow becomes periodic in the wake region for blockage ratio of 1/4. According to Sohankar et al. (1995), the value of critical Reynolds number was found between 50 and 55.

Breuer M. et al. (2000) found the unsteadiness at Re=60.0 for the square cylinder centrally placed in plane channel for blockage ratio of 1/8.

As concluded by Okajima (1982) and Franke (1991) in the Reynolds number range 100-150, the flow past square cylinders can be considered as two-dimensional. In contrast to the circular cylinder flow for which Williamson (1996) provides a Reynolds number limit ($\approx$180) for the onset of three-dimensional structures in the wake, no such clear statement can be found for the square counterpart. A rough hint has been given by Franke (1991) with $Re \leq$ 300. Therefore, beyond this limit three-dimensional structures are expected and subsequently transition to turbulence takes place. So for the present study, the steady flow of power law fluids past square cylinder placed in rectangular channel, the Re=50.0 was chosen as the upper limit.

To analyze the flow researchers have used different approaches. For the solution of poisson equations for pressure, one compatibility condition has to be satisfied. For the staggered-grid this condition is automatically satisfied, however this is not the case for the non-staggered grid. Abdallah S. (1987) proposed the consistent finite difference method by ensuring the satisfaction of compatibility condition on the non-staggered grid.

The no-slip boundary condition applied to the steady, viscous, incompressible flow over a rectangular re-entrant corner boundary leads to singularity in the vorticity and pressure fields. Different methods to handle this problem proposed by different researchers have been summarized and compared by Holstein H. at el. (1981). He shows that discontinuous method and Kawaguti method give the good results as compared to others.

It is thus safe to conclude that there are no prior results available on the confined flow of non-newtonian fluids past a cylinder of square cross-section placed in rectangular channel. This work aims to fill this gap in the literature.

1.3 Objectives of the present work:

In the present work, incompressible and steady flow of Non-Newtonian fluids (power law model) over a square cylinder mounted in a rectangular channel is studied. A finite difference based numerical method Stream function-Vorticity scheme has been used to solve the unsteady Navier-Stocks equations through false transient methodology. The resulting velocity and pressure fields, which are then used to calculate the total, and individual drag coefficients as functions of the Reynolds number, power law index and blockage ratio. Numerical results for different flow parameters, drag coefficients are presented for $5.0 \leq \mathrm{Re} \leq 50.0$ and $1.0 \leq n \leq 1.6$. The present work is limited for study the effect of shear thickening behaviour. The effect of different blockage ratio ($B = 1/8, 1/6, 1/4$) is also reported. Reynolds number and power law index is studied, over a wide range of conditions. A comparison is made with results obtained for the Newtonian fluids to that of the Non-Newtonian fluids to elucidate the effect of Non-Newtonian fluid characteristics.

Chapter 2

PROBLEM FORMULATION

This chapter presents the physical problem studied in this work, followed by its idealization and finally, the mathematical equations describing the flow together with the relevant boundary conditions are presented. The equations are non-dimensionalised in order to reduce the number of variables. Also the auxiliary equations to calculate the viscous drag coefficient, form drag coefficient, non-newtonian viscosity and velocity are presented in this chapter.

2.1 Problem statement:

The present work is concerned with the analysis of the steady, laminar flow of Non-Newtonian fluid (power law model) past square cylinder mounted in a rectangular channel. As mentioned in chapter-1, at low Reynolds number (Re<50.0) the flow is two-dimensional, axisymmetric. Figure (2.1) shows the schematic diagram of the flow model for the present work. Following dimensions (non-dimensionalised with obstacle width) are used:

$$LX = 50.0$$
$$LY = 8.0$$
$$L_a = 12.5$$

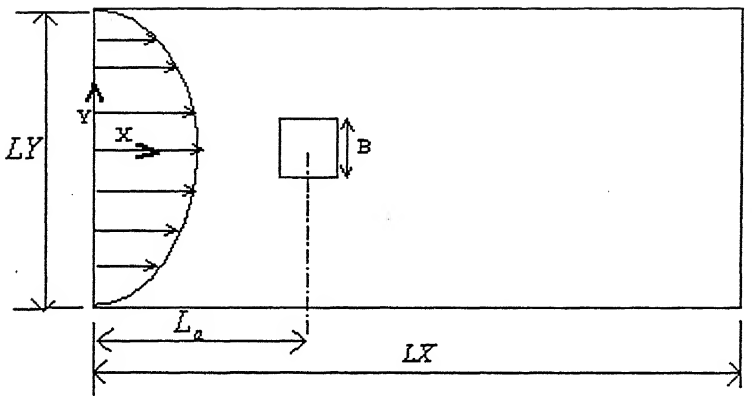

Figure 2.1: Schematic diagram of flow model

2.2 Governing equations:

The governing equations are presented in this section. A rectangular coordinate system is chosen for convenience as shown is figure (2.1). The velocity components in x & y direction are U, V respectively. The flow is two-dimensional and steady. The flow variables do not depend upon the third direction.

Therefore, the velocity components in x-, y- & z- direction are given as

$U'=U'(X',Y')$, $V'=V'(X',Y')$ and $W'=0.0$

Under these conditions the continuity equation for an incompressible reduces to

$$\frac{\partial U'}{\partial X'}+\frac{\partial V'}{\partial Y'}=0.0 \qquad (2.1)$$

And the corresponding x- and y- components of Cauchy equations in stress tensor form are written as:

x-component:

$$\rho\left(\frac{\partial U'}{\partial t'}+U'\frac{\partial U'}{\partial X'}+V'\frac{\partial U'}{\partial Y'}\right)=-\frac{\partial P'}{\partial X'}+\left(\frac{\partial \tau'_{XX}}{\partial X'}+\frac{\partial \tau'_{XY}}{\partial Y'}\right) \qquad (2.2)$$

y-component:

$$\rho\left(\frac{\partial V'}{\partial t'}+U'\frac{\partial V'}{\partial X'}+V'\frac{\partial V'}{\partial Y'}\right)=-\frac{\partial P'}{\partial Y'}+\left(\frac{\partial \tau'_{XY}}{\partial X'}+\frac{\partial \tau'_{YY}}{\partial Y'}\right) \tag{2.3}$$

From the Newton's law of viscosity for an incompressible fluid the stress can be expressed as:

$$\tau=\mu\Delta \tag{2.4}$$

Here,

μ =Coefficient of viscosity

Δ =Rate of deformation tensor

And it is formulated by

$$\Delta_{i,j}=\left(\frac{\partial U_i}{\partial X_j}+\frac{\partial V_j}{\partial Y_i}\right) \tag{2.5}$$

The coefficient of viscosity depends on the local pressure and temperature but not on τ or Δ. For the Non-Newtonian fluids the relationship between $\tau \& \Delta$ is not the simple proportionality given by equation (2.4)

For the certain types of the Non-Newtonian fluid,

$$\tau=\eta\Delta \tag{2.6}$$

Here,

η =Non-Newtonian viscosity

The assumption of various empirical functions to describe the dependence of η on Δ (or η on τ) corresponds to the various models.

The simplest type of the model is power law model, in which the non-newtonian fluid is characterized by two parameters n,m power law index, flow consistency index respectively.

Power law model:

$$\tau = \left\{ m \left| \sqrt{\frac{1}{2}(\Delta : \Delta)} \right|^{(n-1)} \right\} \Delta \tag{2.7}$$

Here,

$$\Delta : \Delta = \sum_i \sum_j \Delta_{i,j} \Delta_{j,i} \tag{2.8}$$

If we assume that

$$\eta = mA \tag{2.9}$$

where,

$$A = \left| \sqrt{\frac{1}{2}(\Delta : \Delta)} \right|^{(n-1)}$$

Then stress can be represented as:

$$\tau = mA\Delta \tag{2.10}$$

Non-dimensionalisation of equations:

For the non-dimensionalisation of the velocity terms the maximum velocity at inflow plane (U_{MAX}) is used, for the length terms the obstacle width (B) is used, for the pressure term $\rho U^2{}_{MAX}$ is used.

Following scaling is used for the non-dimensionalisation of equations.

$$X = \frac{X'}{B} \quad , \quad Y = \frac{Y'}{B} \quad , \quad U = \frac{U'}{U_{MAX}} \quad , \quad V = \frac{V'}{U_{MAX}} \quad ,$$

$$\psi = \frac{\psi'}{U_{MAX} B} \quad , \quad \omega = \frac{\omega' B}{U_{MAX}} \quad , \quad P = \frac{P'}{\rho \, U^2{}_{MAX}}$$

$$\tau = \frac{\tau'}{\rho \, U^2{}_{MAX}} \quad , \quad A = A' \left(\frac{B}{U_{MAX}} \right)^{n-1}$$

The definitions of stress tensor from the power law model equation (2.10) is substituted in equations (2.3) & (2.4) and after the non-dimensionalisation of the resultant equations we get the following equations for the power law fluid.

x-component:

$$\frac{\partial U}{\partial t}+U\frac{\partial U}{\partial X}+V\frac{\partial U}{\partial Y}=-\frac{\partial P}{\partial X}+\frac{1}{\mathrm{Re}}\left[A\left(\frac{\partial^2 U}{\partial X^2}+\frac{\partial^2 U}{\partial Y^2}\right)+2\frac{\partial U}{\partial X}\frac{\partial A}{\partial X}+\left(\frac{\partial U}{\partial Y}+\frac{\partial V}{\partial X}\right)\frac{\partial A}{\partial Y}\right] \quad (2.11)$$

y-component:

$$\frac{\partial V}{\partial t}+U\frac{\partial V}{\partial X}+V\frac{\partial V}{\partial Y}=-\frac{\partial P}{\partial Y}+\frac{1}{\mathrm{Re}}\left[A\left(\frac{\partial^2 V}{\partial X^2}+\frac{\partial^2 V}{\partial Y^2}\right)+2\frac{\partial V}{\partial Y}\frac{\partial A}{\partial Y}+\left(\frac{\partial U}{\partial Y}+\frac{\partial V}{\partial X}\right)\frac{\partial A}{\partial X}\right] \quad (2.12)$$

Here Reynolds number is defined in following way,

$$\mathrm{Re}=\frac{U_{MAX}^{2-n}B^n\rho}{m} \quad (2.13)$$

By cross-differentiation of the above two equations (2.11) & (2.12) and subtraction gives the Vorticity transport equation.

Vorticity transport equation:

$$\frac{\partial \omega}{\partial t}+\frac{\partial}{\partial X}(U\omega)+\frac{\partial}{\partial Y}(V\omega)=\frac{1}{\mathrm{Re}}\left[A\frac{\partial^2\omega}{\partial X^2}+A\frac{\partial^2\omega}{\partial Y^2}+\left(\frac{\partial^2 A}{\partial X^2}-\frac{\partial^2 A}{\partial Y^2}\right)\left(\frac{\partial^2\psi}{\partial Y^2}-\frac{\partial^2\psi}{\partial X^2}\right)+2\frac{\partial A}{\partial X}\frac{\partial\omega}{\partial Y}+2\frac{\partial A}{\partial Y}\frac{\partial\omega}{\partial X}\right.$$
$$\left.-\frac{4}{\mathrm{Re}}\frac{\partial^2 A}{\partial X\partial Y}\frac{\partial^2\psi}{\partial X\partial Y}\right] \quad (2.14)$$

From the definition of vorticity, stream function elliptic equation is formulated.

Stream function elliptic equation:

$$\frac{\partial^2\psi}{\partial X^2}+\frac{\partial^2\psi}{\partial Y^2}=-\omega \quad (2.15)$$

When the equations (2.11) & (2.12) are differentiated with respect to x and y

respectively and added, we get the pressure poisson equation.

$$\frac{\partial^2 p}{\partial X^2}+\frac{\partial^2 P}{\partial Y^2}=\frac{\partial}{\partial X}(V\omega)-\frac{\partial}{\partial Y}(U\omega)+\frac{2}{\mathrm{Re}}\left[\frac{\partial\omega}{\partial X}\frac{\partial A}{\partial Y}-\frac{\partial\omega}{\partial Y}\frac{\partial A}{\partial X}+\frac{\partial U}{\partial X}\frac{\partial^2 A}{\partial X^2}+\frac{\partial V}{\partial Y}\frac{\partial^2 A}{\partial Y^2}+\frac{\partial^2 A}{\partial X\partial Y}\left(\frac{\partial U}{\partial Y}+\frac{\partial V}{\partial X}\right)\right] \quad (2.16)$$

Equations (2.14), (2.15) & (2.16) are solved numerically to get the solution.

2.3 Initial and boundary conditions:

The numerical calculations are started with initial guess for all the flow field variables over the entire physical domain. Firstly the results were calculated for Newtonian fluids ($n=1.0$) with different initial guesses and all led to same flow field. The best initial guess is that with which the code converges fastest and gives the solution. For the Newtonian fluids, fully developed velocity field solution gives the fastest convergence. For the Non-Newtonian fluids the calculations are started with solution of Newtonian fluids as an initial guess.

The present problem is solved with stream function-vorticity method. So first the boundary conditions are modeled for velocity, and then those boundary conditions are formulated for stream function and vorticity. The following boundary conditions are used:

For the momentum equations:

- Inflow plane: Parabolic profile has been used for the velocity.

$$U=U(Y)=\left[1-\left(\frac{Y}{LY/2}\right)^{\left(\frac{n+1}{n}\right)}\right], \quad V=0.0$$

for the stream function:

$$\psi = \left[Y - \frac{n}{2n+1} \left(\frac{2}{LY} \right)^{\left(\frac{n}{n+1}\right)} Y^{\left(\frac{2n+1}{n}\right)} \right]$$

Physically no boundary condition is available for vorticity. So vorticity at inflow plane is calculated numerically by equation (2.15).

- Out flow: There is no unique prescription for the out flow condition. The idea is to have specification that would not affect the flow in the upstream. So fully developed boundary condition is used.

  $$V = 0.0 \quad , \quad \frac{\partial U}{\partial X} = 0.0$$

  for the stream function and vorticity:

  $$\frac{\partial \psi}{\partial X} = 0.0 \quad , \quad \frac{\partial \omega}{\partial X} = 0.0$$

- Confining boundary (channel wall): No-slip boundary condition is used

  $$U = 0.0 \quad , \quad V = 0.0$$

  Stream function value at the lower wall:

  $$\psi = -\frac{n+1}{2n+1} \frac{LY}{2.0}$$

  Stream function value at the upper wall:

  $$\psi = \frac{n+1}{2n+1} \frac{LY}{2.0}$$

- Obstacle: No- slip boundary condition is used.

  $$U = 0.0 \quad , \quad V = 0.0$$

  $$\psi = 0.0$$

No physical boundary condition is available for vorticity at the walls. So the vorticity is calculated numerically by equation (2.15) at all the solid walls.

For the pressure solution: The pressure boundary conditions are found out from the momentum equations.

- At x=constant boundary

$$\frac{\partial P}{\partial X} = V\omega - \frac{A}{\mathrm{Re}}\frac{\partial \omega}{\partial Y} + \frac{1}{\mathrm{Re}}\left(2\frac{\partial U}{\partial X}\frac{\partial A}{\partial X} + \frac{\partial U}{\partial Y}\frac{\partial A}{\partial Y} + \frac{\partial V}{\partial X}\frac{\partial A}{\partial Y}\right)$$

- At y=constant boundary

$$\frac{\partial P}{\partial Y} = -U\omega - \frac{A}{\mathrm{Re}}\frac{\partial \omega}{\partial X} + \frac{1}{\mathrm{Re}}\left(2\frac{\partial V}{\partial Y}\frac{\partial A}{\partial Y} + \frac{\partial U}{\partial Y}\frac{\partial A}{\partial X} + \frac{\partial V}{\partial X}\frac{\partial A}{\partial X}\right)$$

2.4 Calculation of Drag:

After solving equations (2.14), (2.15) and (2.16) numerically to obtain the velocity field and pseudo-pressure field, the results are used to estimate the individual components of drag coefficient. The drag coefficient represents the rate of energy dissipation due to the tangential and normal forces acting on the surface of the solid cylinder. Therefore, the total drag comprises of individual components, i.e., friction drag due to shear stress and pressure or form drag due to pressure.

The drag coefficient is defined as:

$$C_D = \frac{F_D}{\frac{1}{2}\rho U^2{}_{MAX} L} \tag{2.17}$$

Here F_D is the drag force exerted by the fluid on the cylinder. L represents the length in the third direction, as we are solving problem as a two-dimensional, so unit length is assumed. Both parts of drag are calculated separately and then added.

Viscous drag coefficient: This part is calculated by integrating the shear force at the upper and lower surface of the cylinder

$$C_{D_f} = \frac{2}{\mathrm{Re}} \int_{LS} \left(A \frac{\partial U}{\partial Y} \right) dx + \frac{2}{\mathrm{Re}} \int_{US} \left(A \frac{\partial U}{\partial Y} \right) dx \qquad (2.18)$$

LS: Lower surface

US: Upper surface

Form drag coefficient: This part is calculated by integrating the pressure at the front and rear side of cylinder.

$$C_{D_p} = 2 \left[\int_1 P(Y) dy - \int_2 P(Y) dy \right] \qquad (2.19)$$

1: Front side of the cylinder

2: Rear side of the cylinder

Here $P(Y)$ is the non-dimensional pressure distribution over the cylinder.

2.5 Calculation of Non-Newtonian viscosity:

As we have discussed that non-newtonian viscosity can be represented as

$\eta = mA$

After the non-dimensionalisation of the equations only 'A' term has to be calculated, this is calculated by the following equation:

$$A = \left| \sqrt{4 \left(\frac{\partial^2 \psi}{\partial X \partial Y} \right)^2 + \left(\frac{\partial^2 \psi}{\partial Y^2} - \frac{\partial^2 \psi}{\partial X^2} \right)^2} \right|^{n-1}$$

2.6 Calculation of velocity:

After solving the equations in terms of vorticity and stream function, the velocity component are calculated by the following equations:

$$U = \frac{\partial \psi}{\partial Y}$$

$$V = -\frac{\partial \psi}{\partial X}$$

Chapter 3

Description of numerical technique

Fluid flow can be modeled using the principles of conservation of mass and Newton's second law of motion. These laws can be developed in form of partial differential equations along with the suitable boundary conditions. These differential equations are non-linear and do not admit analytical solutions. Numerical approach is the practical alternative for analyzing the flow problem.

Extensive study has been carried out in the recent decades for developing numerical schemes to solve incompressible Navier-Stocks equations in regular and multi-dimensional complex geometries. The main difficulty with the incompressible flow simulation is the absence of an obvious equation for pressure. Specifically the nature of coupling of velocity and pressure variables is implicit in nature. When the flow is treated as incompressible, pressure does not have the usual thermodynamic meaning. Here it has a relative value, which adjusts itself instantaneously in such a way that the condition of zero divergence is satisfied at all computational grid points. This behaviour is related to the fact that the speed of sound becomes infinite in an incompressible fluid. As a consequence, the pressure field cannot be calculated by a time-advancement procedure. Instead it requires at least one partially implicit determination, which is able to take in to account the coupling between the pressure and velocity fields, subject to the boundary conditions.

3.1 Resolution of pressure and velocity coupling:

The difficulties associated with the determination of pressure have led to the methods that eliminate pressure from the governing equations. Some methods are available to solve the incompressible equations. One of the popular methods for solving the incompressible Navier-Stocks equations involves replacing the primitive variables with stream function and vorticity. If the problem is limited to two-dimensional, this method can be applied successfully and easily. The elimination of pressure by cross differentiation of two momentum equations leads to the vorticity transport equation. This equation when combined with the definition of vorticity leads to the basis of stream function-vorticity method. In order to determine the pressure at each grid points, it is necessary to solve an additional equation, which is referred to as the poisson equation for the pressure. Differentiation of equation (2.11) with respect to x and differentiation of equation (2.12) with respect to y and add of the results gives the poisson equation for pressure.

3.2 Method of solution:

The governing equations in each case have been solved on a non-staggered grid by using stream function-vorticity method. Since the present work is limited to low Reynolds number ($5.0<Re<50.0$), in this regime the fluid does not show any three-dimensionality in the flow, so the present work is limited by two-dimensional flow simulation. Among the available methods stream function- vorticity method was chosen for the flow simulation because this method can be applied easily and successfully for two-dimensional simulation.

Three equations vorticity transport equation, stream function elliptic

equation and pressure poisson equation have to be solved. Since the problem is steady, so first the vorticity transport equation and the stream function equation are solved simultaneously to get steady state solution for velocity through false transient method. Then the steady state velocity solution is used to solve the pressure poisson equation for the pressure. The velocity field and pressure field are used to find out individual drag coefficients. The flow chart for the complete solution is given in figure (3.3)

3.2.1 Velocity solution:

The pseudo-unsteady method is used to solve the vorticity transport equation with the elliptic stream function equation. In this method the steady problem is treated as unsteady problem, the unsteady incompressible equations are solved numerically to achieve the steady solutions through convergence. For the convective term of the vorticity transport equation, second order upwind scheme has been used. Diffusion terms of the vorticity transport equation have been approximated by second order central difference. The same second order difference scheme have been employed for the second order derivative in the stream function elliptic equation

Following algorithm is used to get velocity solution:

- Specify initial values for stream function and vorticity at time $t = 0.0$
- Solve the vorticity transport equation for vorticity at each interior grid points at $t + \Delta t$
- Iterate the new stream function value at all points by solving the elliptic equation using new vorticity values at interior points.
- Find the velocity components from

$$U = \frac{\partial \psi}{\partial Y} \ , \ V = -\frac{\partial \psi}{\partial X}$$

- Determine values of vorticity on the boundaries using new value of stream function and vorticity at interior points.
- Return to step 2 if the solution is not converged

3.2.2 Pressure solution:

Solution for the pressure is obtained from the poisson equation (divergence of the momentum equation) with the Neumann boundary conditions. Solution for the poisson equation exists only if a compatibility condition is satisfied. This condition relates the source of poisson equation (2.16) and the Neumann boundary conditions (Green's theorem).

$$\int_{x=0}^{1}\int_{y=0}^{1} \sigma \, dxdy = \int P_{nb} dS$$

Here,

σ : Source term of the poisson equation (2.16)

nb :Outward normal to boundary contour S, enclosing the solution domain

This compatibility condition is not automatically satisfied on the non-staggered grid. Failure to satisfy the compatibility condition leads to non-convergent iterative solutions. A number of methods are available by ensuring the convergence. In the present work a method developed by Abdallah S. (1986) has been used. Consistent finite difference approximations for the pressure equation with Neumann boundary conditions have been developed to exactly satisfy the compatibility. He developed the scheme for the equations for the Newtonian fluids. That scheme has been modified for the Non-Newtonian fluids (power law model). Here some outlines of that method for the Newtonian fluids with the specified grid arrangement are presented.

Consistent Finite Difference approximations: Following finite difference grid arrangement is used for this scheme.

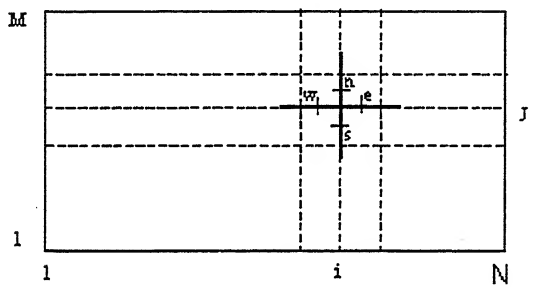

Figure 3.1: Grid arrangement for solution of pressure poisson equation

Pressure poision equation for the Newtonian fluid is written as:

$$P_{XX} + P_{YY} = (V\omega)_X - (U\omega)_Y$$

The subscripts x, y refer to the partial derivatives with respect to x, y.

The equation is approximated at grid points (i, j) using second order accurate formulas in the following way:

$$(P_X - V\omega)_e - (P_X - V\omega)_w + (P_Y + U\omega)_n - (P_Y + U\omega)_s = 0.0$$

e, w, n, s are the mid points on the lines joining the grid points.

The pressure gradients P_X and P_y are approximated using second order accurate formulas at the locations e, w, n, s as

$$(P_X)_w = (P_{i,j} - P_{i-1,j})/h$$

$$(P_X)_e = (P_{i+1,j} - P_{i,j})/h$$

$$(P_X)_s = (P_{i,j} - P_{i,j-1})/h$$

$$(P_X)_n = (P_{i,j+1} - P_{i,j})/h$$

h : grid spacing (uniform in both direction)

The values of velocity and vorticity at e, w, n, s are calculated from their values at the grid locations by averaging

$$V_w = \left(V_{i,j} + V_{i-1,j}\right)/2.0$$

For consistency, the pressure gradients P_X is evaluated at the location $x = \frac{1}{2}$ and not at $x = 0.0$. All the pressure gradients are evaluated not at the exact boundary grid points, but at the point that is middle of boundary grid point and the next grid point to boundary grid point in the domain. By using this approximation, the compatibility condition is satisfied.

3.3 Grid system:

The computational domain is divided into set of rectangular cells and a non-staggered arrangement is used such that all variables are defined at the corners of the cells. Grid points exactly lies on the cylinder surface. Two-dimensional simulation has been carried out on uniform grids and grid independence study has been discussed in chapter-4.

3.4 Finite Difference Discretization:

The present problem has been solved with the finite difference based methodology. In this method, the derivatives in the partial differential equations are replaced by finite difference quotients derived from the Taylor series expression. The time derivative is discritized explicitly. For the convective term of the vorticity transport equation, second order upwind scheme has been used. Diffusion terms of the vorticity transport equation have been approximated by second order central difference.

Second order upwind scheme: The following Discretization (sample) is used in the second order upwind scheme.

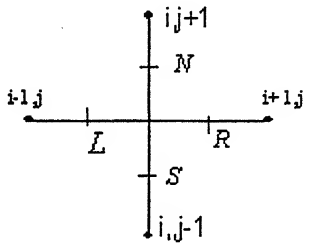

Figure 3.2: Grid arrangement for the second order upwind scheme

$$\frac{d}{dX}(U\omega)=\frac{U_R\omega_R-U_L\omega_L}{DX}$$

Here,

$$U_R=\frac{U_i+U_{i+1}}{2}$$

$$U_L=\frac{U_i+U_{i-1}}{2}$$

if $U_R>0.0$ then $\omega_R=\omega_i$

if $U_R<0.0$ then $\omega_R=\omega_{i+1}$

if $U_L>0.0$ then $\omega_L=\omega_{i-1}$

if $U_L<0.0$ then $\omega_L=\omega_i$

The discritization of vorticity transport equation (2.14) is presented here.

$$\frac{\omega_{i,j}^{n+1}-\omega_{i,j}^{n}}{\Delta t}+\frac{U_R\omega_R-U_L\omega_L}{\Delta X}+\frac{U_S\omega_S-U_N\omega_N}{\Delta Y}=\frac{A_{i,j}^{n}}{\mathrm{Re}}\frac{\omega_{i+1,j}^{n}-2\omega_{i,j}^{n}+\omega_{i-1,j}^{n}}{\Delta X^2}+\frac{A_{i,j}^{n}}{\mathrm{Re}}\frac{\omega_{i,j+1}^{n}-2\omega_{i,j}^{n}+\omega_{i,j-1}^{n}}{\Delta Y^2}$$

$$+\frac{1}{\mathrm{Re}}\left(\frac{A_{i+1,j}^{n}-2A_{i,j}^{n}+A_{i-1,j}^{n}}{\Delta X^2}-\frac{A_{i,j+1}^{n}-2A_{i,j}^{n}+A_{i,j-1}^{n}}{\Delta Y^2}\right)\left(\frac{\psi_{i,j+1}^{n}-2\psi_{i,j}^{n}+\psi_{i,j-1}^{n}}{\Delta Y^2}-\frac{\psi_{i+1,j}^{n}-2\psi_{i,j}^{n}+\psi_{i-1,j}^{n}}{\Delta X^2}\right)$$

$$+\left(2\frac{A_{i+1,j}^{n}-A_{i-1,j}^{n}}{2\Delta X}\frac{\omega_{i+1,j}^{n}-\omega_{i-1,j}^{n}}{2\Delta X}\right)+\left(2\frac{A_{i,j+1}^{n}-A_{i,j-1}^{n}}{2\Delta Y}\frac{\omega_{i,j+1}^{n}-\omega_{i,j-1}^{n}}{2\Delta Y}\right)$$

$$-4\left(\frac{A_{i+1,j+1}^{n}+A_{i-1,j-1}^{n}-A_{i-1,j+1}^{n}-A_{i+1,j-1}^{n}}{4\Delta X\Delta Y}\frac{\psi_{i+1,j+1}^{n}+\psi_{i-1,j-1}^{n}-\psi_{i-1,j+1}^{n}-\psi_{i+1,j-1}^{n}}{4\Delta X\Delta Y}\right)$$

3.5 Treatment of corner points:

The corner point treatment is very much important. It is well known that the no-slip, plane, viscous, incompressible fluid flow over a rectangular re-entrant corner boundary leads to a singularity in the vorticity and the pressure fields. The presence of the singularity implies that the stream function and vorticity do not have Taylor series expansion in the regions that include corners. Consequently the usual discritization methods cannot be applied. Two methods Kawaguti method and discontinuous method were tried and there were no so much effective variations in the results. The results, which are reported here, are based on discontinuous method. In the discontinuous method, at the corner point two values are calculated for the vorticity and pressure obtained from the both (x- and y-) direction equations.

3.6 Numerical stability:

For accuracy, the mesh size must be small enough to resolve the expected spatial variation in all the dependent variables. But the usage of very fine grid makes the calculation very expensive. So on the basis of grid independence test, a proper mesh size is chosen. Once the mesh has been chosen, the condition on the time step necessary to prevent numerical instabilities are determined from the combination of CFL (Courant-Friedriches-Law) condition and the restriction on the grid Fourier number. According to CFL condition, the distance the fluid travels in one time increment must be less then one space increment. This leads to a constraint on the time step in the form

$$\Delta t < \left\{ \frac{\Delta X}{|U|}, \frac{\Delta Y}{|V|}, \right\}$$

When the viscous diffusion terms are important, the condition necessary to ensure stability is dictated by the restriction on the grid Fourier number and can be shown to be

$$\Delta t < \frac{RE}{2.0} \left\{ \frac{\Delta X^2 \Delta Y^2}{\Delta X^2 + \Delta Y^2} \right\}$$

The final time step is the minimum of the values obtained from.

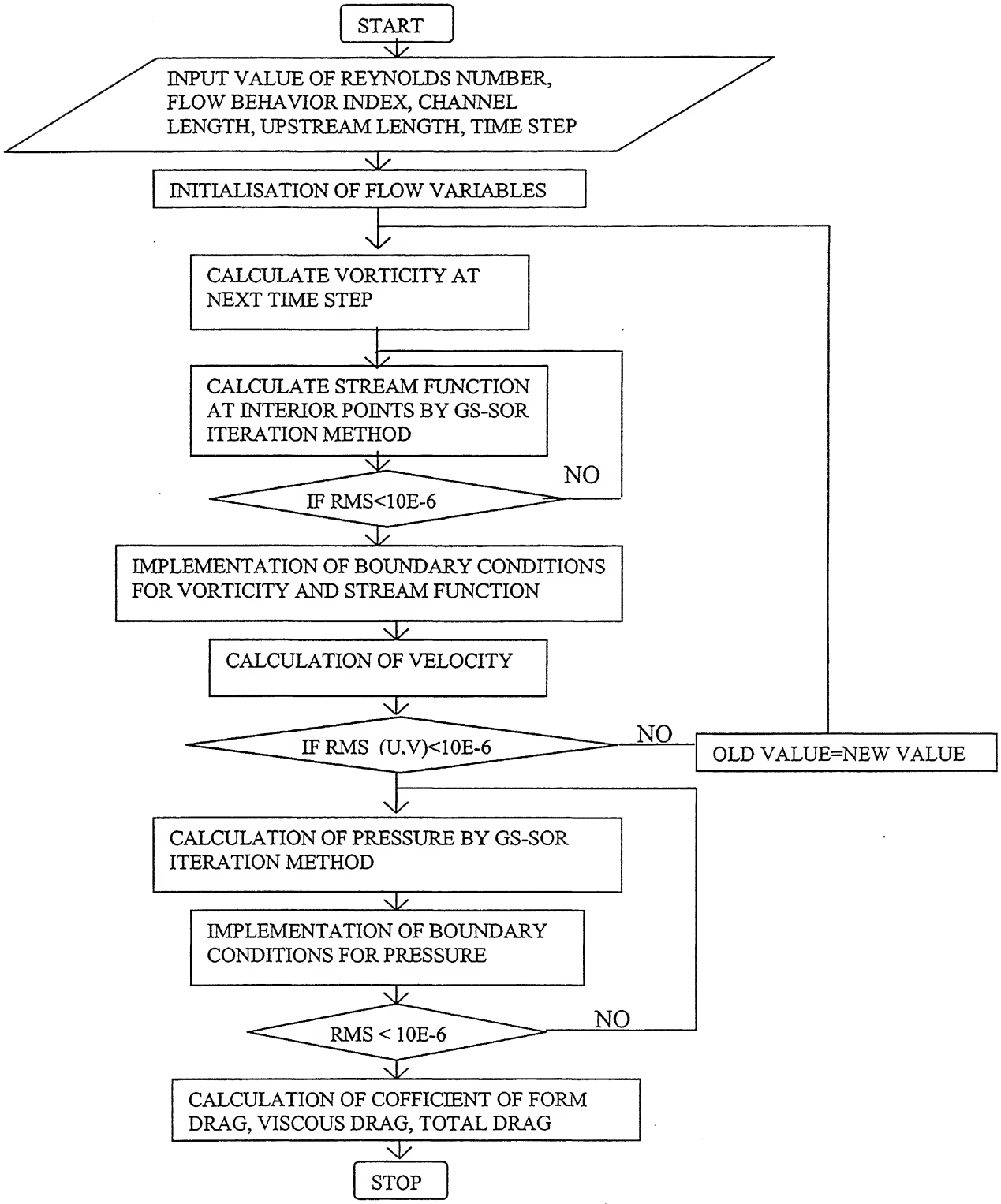

Figure 3.3: Flow chart for the solution of problem

Chapter-4

Results and Discussion

The flow of Non-Newtonian fluids (power law model) past a square cylinder placed in a rectangular channel has been analyzed in the present work. The present study has been done in the low Reynolds number range ($5.0 \leq \mathrm{Re} \leq 50.0$). The streamlines patterns, iso-vorticity patterns, recirculation length, individual coefficient of drags have been computed numerically. The present study is concerned with the shear-thickening fluids or dilantant fluids ($n > 1.0$). In the present work, study has been done for $1.0 \leq n \leq 1.6$. The effect of the blockage ratio ($B = 1/8,1/6,1/4$) has also been reported. The numerical results are presented and discussed in this chapter.

Time-step used in the problem first was calculated as described in section 3.6.The final time-step used in the problem varies with the different parameters such as Reynolds number, power law index, and blockage ratio. For $B = 1/8$, $n = 1.0$ and $\mathrm{Re} = 50.0$ case, Δt (time step)=0.001 was used. For the lower value of Reynolds number ($\mathrm{Re} < 50.0$) and for $n > 1.0$, further lower value of the time-step was used as compared to upper given value.

4.1 Grid Independence Test:

Three different spatial grid spacing (uniform and same in both direction) ($\Delta x = 0.2,0.1,0.05$) were used and results were compared for the one case. The following figure 4.1 shows the effect of the different spatial grid spacing.

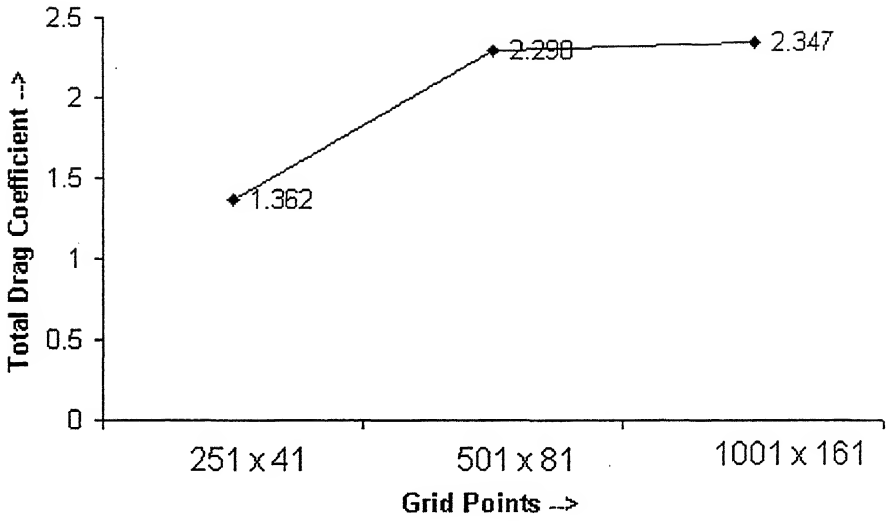

Figure 4.1 Grid independence test ($\mathrm{Re} = 20.0, B = 1/8, n = 1.0$)

There is not much difference between results obtained with $\Delta x = \Delta y = 0.1(501x81)$ & $\Delta x = \Delta y = 0.05(1001x161)$, but the time taken by the code with finest grid $\Delta x = \Delta y = 0.05$ (1001x161) was very much as compared to that of $\Delta x = \Delta y = 0.1$(501x81), so finally $\Delta x = \Delta y = 0.1$ (501x81) uniform grad spacing was chosen for solving the present problem numerically.

4.2 Streamlines and Iso-vorticity Plots:

Streamlines and iso-vorticity plots provide useful information about the detailed kinematics of the fluid flow. These plots provide the qualitative information about the flow. Streamlines contour plots show the separation of the flow, reattachment in the flow and recirculation region. Some representive stream function and vorticity plots have been presented herein. Different plots have been categorized in the following way:

4.2.1 Effect of the blockage ratio:

Figure 4.2 to 4.4 shows the streamlines patterns corresponding to $B = 1/8, 1/6, 1/4$ at $n = 1.0$ and $\mathrm{Re} = 50.0$.

4.2.2 Effect of the Reynolds number:

In this section streamlines patterns figure 4.5 to 4.7 have been drawn to show the effect of Reynolds number at constant value of power law index $n = 1.2$ & blockage ratio $B = 1/8$. It is clear from figure 4.4 to 4.7 (corresponding to $\mathrm{Re} = 10.0, 20.0, 50.0$ Respectively) that as the Reynolds number increases; the length of recirculation region increases.

4.2.3 Effect of the power law index:

Figure 4.8 to 4.11 shows the streamlines patterns corresponding to $n = 1.0, 1.2, 1.4, 1.6$ at $\mathrm{Re} = 50.0$ and $B = 1/6$. These plots have been drawn to show the effect of power law index. Similarly figure 4.12 to 4.15 shows the iso-vorticity plots corresponding to $n = 1.0, 1.2, 1.4, 1.6$ respectively for $B = 1/6$ and $\mathrm{Re} = 50.0$.

4.3 Recirculation Length:

For the flow problems at steady state, the recirculation length is also important parameter. Recirculation length for the square cylinder has been computed numerically. This parameter has been computed as a function of Reynolds number, power law index, and blockage ratio. Some representive values have been summarized in the following tables to show the effect of all the three parameters (Re, n, B)

4.3.1 Effect of Reynolds number:

The following table 4.1 shows the recirculation length as a function of Reynolds number at constant value of blockage ratio and power law index.

Table 4.1: Effect of the Reynolds number on the recirculation length

Reynolds Number	Recirculation Length ($B = 1/8 \,\&\, n = 1.2$)
5.0	0.23
10.0	0.50
20.0	1.00
50.0	2.72

It's clear for the above table that as the Reynolds number increases, the recirculation length increases.

4.3.2 Effect of Power law index:

The following table 4.2 shows the recirculation length as a function of power law index at constant value of Reynolds number and blockage ratio.

Table 4.2: Effect of power law index on the recirculation length

Power law index	Recirculation length ($\mathrm{Re} = 50.0 \,\&\, B = 1/8$)
1.0	2.51
1.2	2.72
1.4	2.91
1.6	3.05

It's clear from the table 4.2 that as the value of power law index increases, the recirculation length also increases. But this happens only at lower blockage

ratio ($B = 1/8, 1/6$). It was found that at $B = 1/4$, the recirculation length does not very with respect to power law index much.

4.3.3 Effect of the blockage ratio:

The following table 4.3 shows the effect of blockage ratio on the recirculation length at constant value of Reynolds number and power law index.

Table 4.3: Effect of blockage ratio on recirculation length

Blockage Ratio	Recirculation Length ($\mathrm{Re} = 50.0 \,\&\, n = 1.2$)
1/8	2.72
1/6	2.01
1/4	1.20

It's clear for the table 4.3 that recirculation length decreases with increase in blockage ratio.

4.4 Coefficient of drag:

One of the important characteristic quantities of the flow around the cylinder is the drag coefficient. While the streamlines and iso-vorticity patterns provide information about the kinematics of flow, the drag phenomena provide the overall hydrodynamic picture of the flow. In the region of small Reynolds number the coefficient of drag varies strongly with Reynolds number. The contribution of the viscous and pressure forces to the total force is of the same magnitude. The coefficient of drag has been computed with various parameters. The values of the individual coefficient of drags and the total coefficient of drag are summarized in the following tables with respect to different parameters.

Table 4.4: Viscous, form and total drag coefficient ($B = 1/8, n = 1.0$)

Reynolds Number	Viscous Drag Coefficient (C_{D_f})	Form Drag Coefficient (C_{D_p})	Total Drag Coefficient (C_D)
5.0	1.860	5.225	7.085
10.0	1.019	3.272	4.291
20.0	0.549	2.249	2.798
50.0	0.219	1.588	1.807

Table 4.5: Viscous, form and total drag coefficient ($B = 1/8, n = 1.2$)

Reynolds Number	Viscous Drag Coefficient (C_{D_f})	Form Drag Coefficient (C_{D_p})	Total Drag Coefficient (C_D)
5.0	1.699	2.659	4.348
10.0	0.958	1.823	2.781
20.0	0.536	1.411	1.947
50.0	0.227	1.210	1.427

Table 4.6: Viscous, form and total drag coefficient ($B = 1/8, n = 1.4$)

Reynolds Number	Viscous Drag Coefficient (C_{D_f})	Form Drag Coefficient (C_{D_p})	Total Drag Coefficient (C_D)
5.0	1.618	1.838	3.456
10.0	0.944	1.299	2.243
20.0	0.547	1.058	1.605
50.0	0.245	0.99	1.235

Table 4.7: Viscous, form and total drag coefficient ($B = 1/8, n = 1.6$)

Reynolds Number	Viscous Drag Coefficient (C_{D_f})	Form Drag Coefficient (C_{D_p})	Total Drag Coefficient (C_D)
5.0	1.518	0.962	2.480
10.0	0.924	0.737	1.661
20.0	0.555	0.666	1.221
50.0	0.264	0.704	0.968

Table 4.8: Viscous, form and total drag coefficient ($B = 1/6, n = 1.0$)

Reynolds Number	Viscous Drag Coefficient (C_{D_f})	Form Drag Coefficient (C_{D_p})	Total Drag Coefficient (C_D)
5.0	2.242	6.415	8.657
10.0	1.179	3.825	5.004
20.0	0.618	2.533	3.151
50.0	0.244	1.743	1.987

Table 4.9: Viscous, form and total drag coefficient ($B = 1/6, n = 1.2$)

Reynolds Number	Viscous Drag Coefficient (C_{D_f})	Form Drag Coefficient (C_{D_p})	Total Drag Coefficient (C_D)
5.0	2.162	3.386	5.448
10.0	1.155	2.149	3.304
20.0	0.621	1.595	2.216
50.0	0.260	1.315	1.575

Table 4.10: Viscous, form and total drag coefficient ($B = 1/6, n = 1.4$)

Reynolds Number	Viscous Drag Coefficient (C_{D_f})	Form Drag Coefficient (C_{D_p})	Total Drag Coefficient (C_D)
5.0	2.175	2.353	4.528
10.0	1.184	1.536	2.72
20.0	0.655	1.188	1.843
50.0	0.286	1.070	1.356

Table 4.11: Viscous, form and total drag coefficient ($B = 1/6, n = 1.6$)

Reynolds Number	Viscous Drag Coefficient (C_{D_f})	Form Drag Coefficient (C_{D_p})	Total Drag Coefficient (C_D)
5.0	2.169	1.262	3.421
10.0	1.202	0.862	2.064
20.0	0.680	0.817	1.497
50.0	0.309	0.754	1.063

Table 4.12: Viscous, form and total drag coefficient ($B = 1/4, n = 1.0$)

Reynolds Number	Viscous Drag Coefficient (C_{D_f})	Form Drag Coefficient (C_{D_p})	Total Drag Coefficient (C_D)
5.0	3.396	10.190	13.586
10.0	1.702	5.624	7.326
20.0	0.854	3.437	4.291
50.0	0.332	2.190	2.512

Table 4.13: Viscous, form and total drag coefficient ($B = 1/4, n = 1.2$)

Reynolds Number	Viscous Drag Coefficient (C_{D_f})	Form Drag Coefficient (C_{D_p})	Total Drag Coefficient (C_D)
5.0	3.695	5.956	9.651
10.0	1.858	3.415	5.273
20.0	0.943	2.323	3.175
50.0	0.380	1.643	2.123

Table 4.14: Viscous, form and total drag coefficient ($B = 1/4, n = 1.4$)

Reynolds Number	Viscous Drag Coefficient (C_{D_f})	Form Drag Coefficient (C_{D_p})	Total Drag Coefficient (C_D)
5.0	4.170	4.503	8.673
10.0	2.109	2.602	4.711
20.0	1.083	1.704	2.787
50.0	0.447	1.324	1.771

Table 4.15: Viscous, form and total drag coefficient ($B = 1/4, n = 1.6$)

Reynolds Number	Viscous Drag Coefficient (C_{D_f})	Form Drag Coefficient (C_{D_p})	Total Drag Coefficient (C_D)
5.0	4.667	2.661	7.328
10.0	2.369	1.553	3.992
20.0	1.226	1.023	2.249
50.0	0.516	0.890	1.406

The individual coefficient of drags and total coefficient of drag have been presented in the tabular form for the various parameters. In the next session coefficient of drag will be represented in the graphical form to show the effect of Reynolds number, blockage ratio and power law index.

4.4.1 Effect of Reynolds number and Power law index:

Figure 4.16 to 4.18 have been plotted for Coefficient of Drag v/s Reynolds number for three different blockage ratio (1/8,1/6,1/4). In all the three graphs, the plots have been shown for different values of the power law index (1.0,1.2,1.4,1.6). It's clear from the graph that as the Reynolds number increases by keeping blockage ratio and power law index constant, the coefficient of drag decreases. Similarly at the constant value of blockage ratio and Reynolds number, the coefficient of drag decreases with increase in the power law index or increasing the shear thickening effect.

4.4.2 Effect of Reynolds number and blockage ratio:

Figure 4.19 to 4. 22 have been plotted for coefficient of drag v/s Reynolds number for different values of power law index ($n = 1.0,1.2,1.4,1.6$). In all 4 graphs, the effect of blockage ratio is also presented. It's clear form the graphs that as the blockage ratio increases, the coefficient of drag also increases.

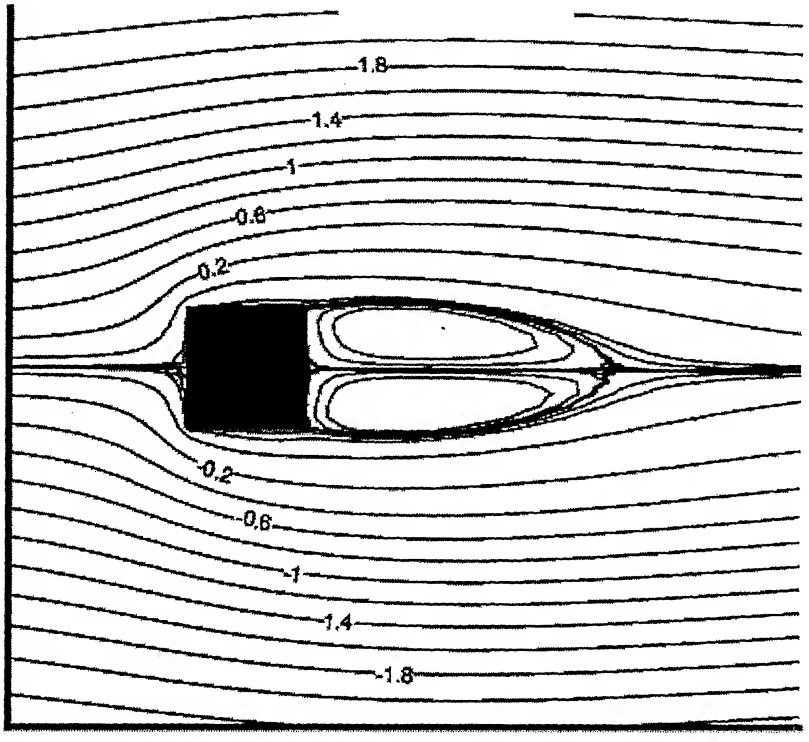

Figure 4.2

Streamlines pattern

Blockage Ratio: 1/8, Reynolds Number: 50.0
Power Law Index: 1.0

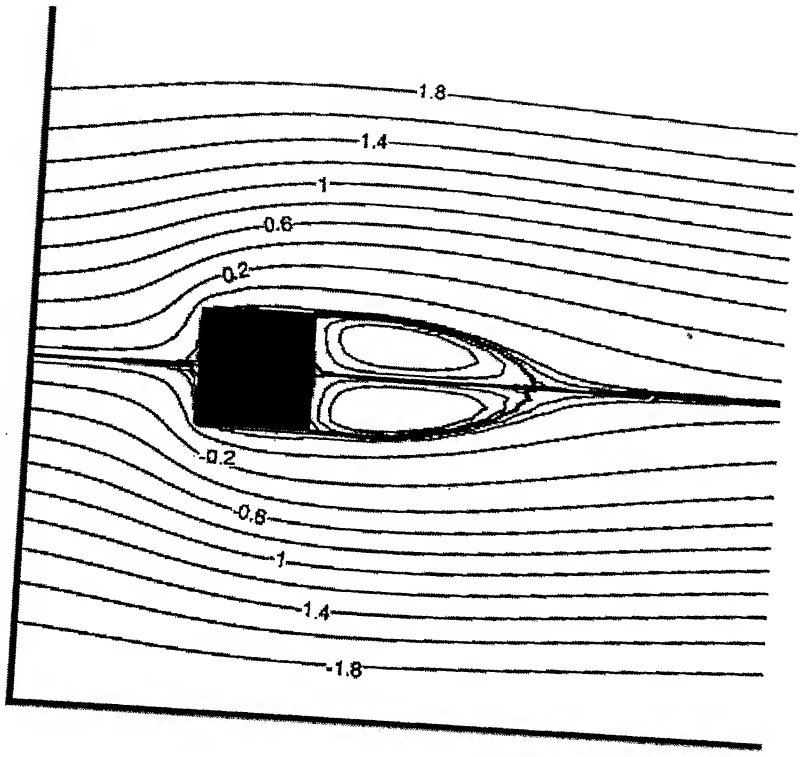

Figure 4.3

Streamlines pattern

Blockage Ratio: 1/6, Reynolds Number: 50.0
Power Law Index: 1.0

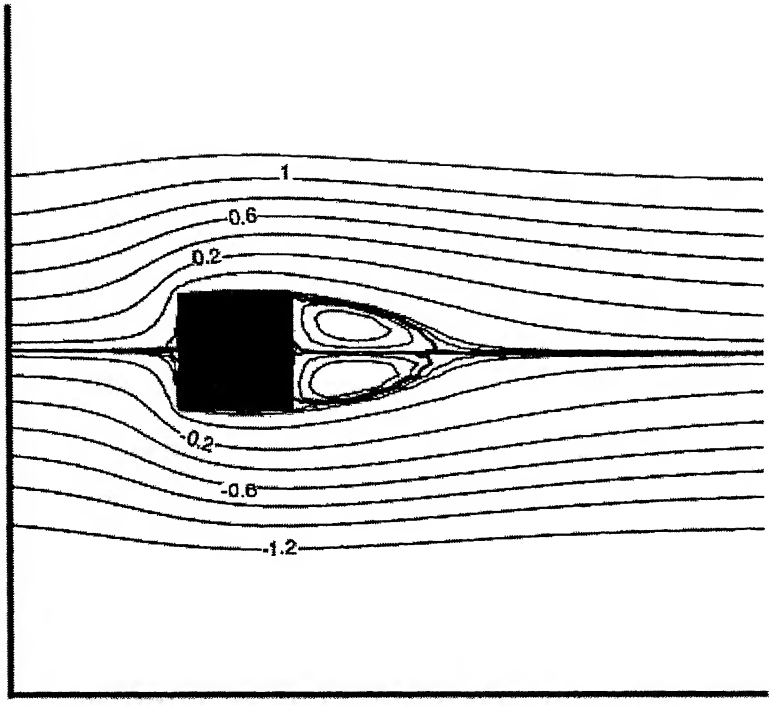

Figure 4.4

Streamlines pattern

Blockage Ratio: 1/4, Reynolds Number: 50.0
Power Law Index: 1.0

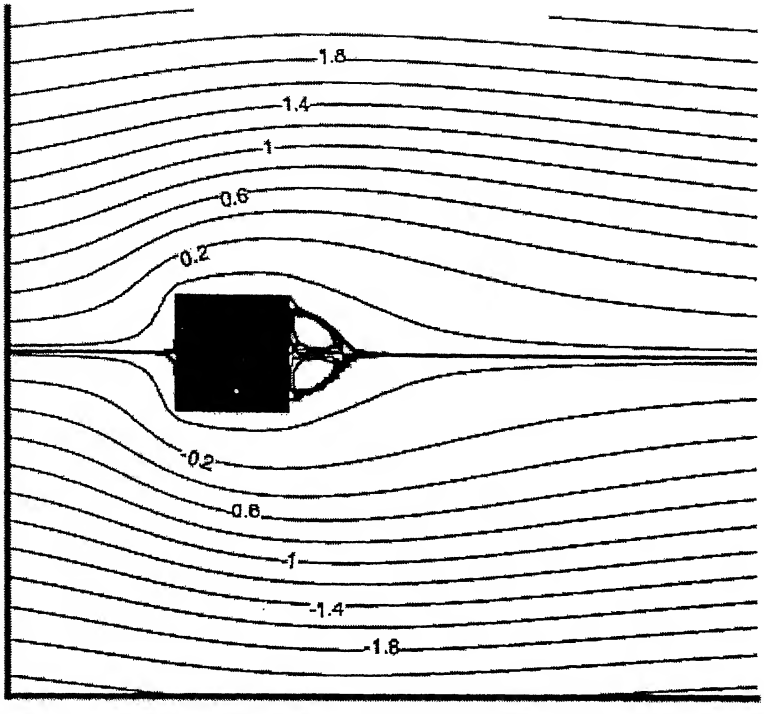

Figure 4.5

Streamlines pattern

Reynolds Number: 10.0, Blockage Ratio:1/8
Power Law Index: 1.2

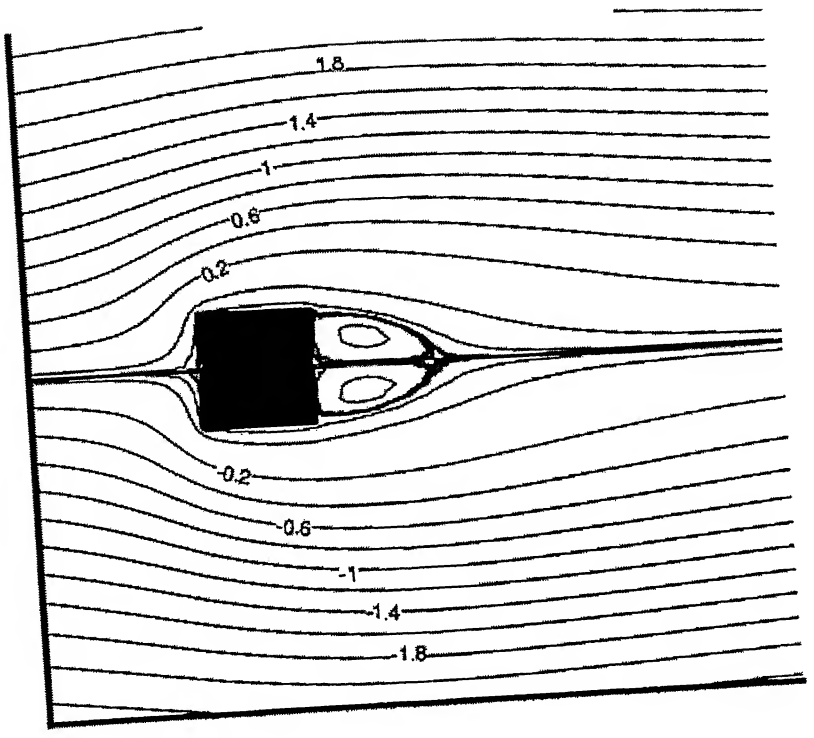

Figure 4.6

Streamlines pattern

Reynolds Number: 20.0, Blockage Ratio:1/8
Power Law Index: 1.2

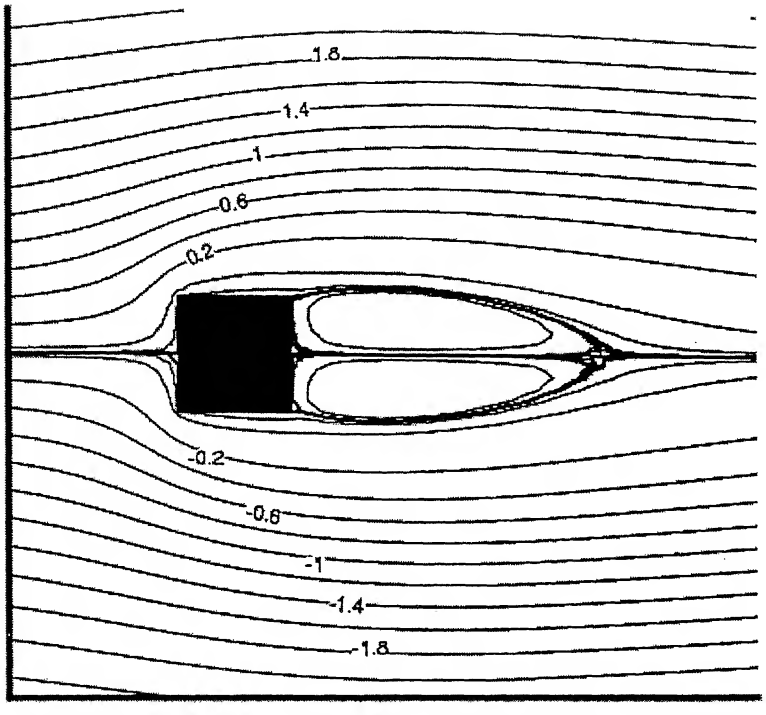

Figure 4.7

Streamlines pattern

Reynolds Number: 50.0, Blockage Ratio:1/8
Power Law Index: 1.2

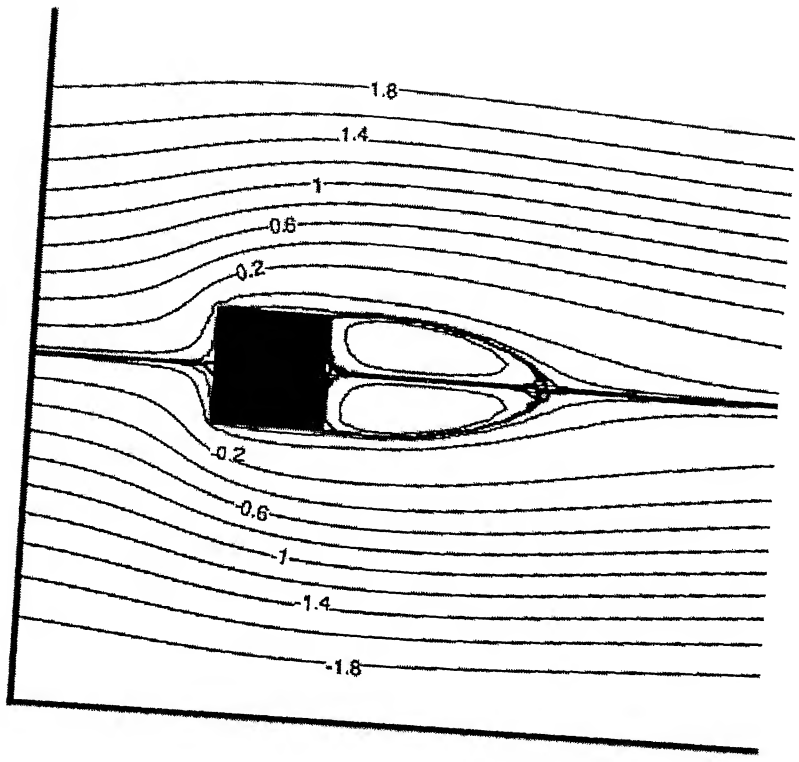

Figure 4.8

Streamlines pattern

Power Law Index: 1.0, Reynolds Number: 50.0, Blockage Ratio: 1/6

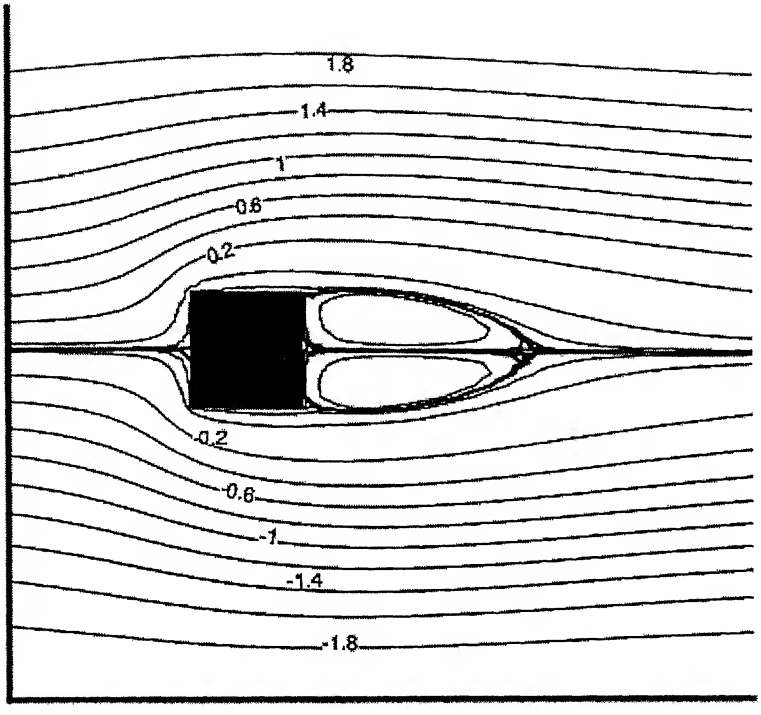

Figure 4.9

Streamlines pattern

Power Law Index: 1.2, Reynolds Number: 50.0,
Blockage Ratio: 1/6

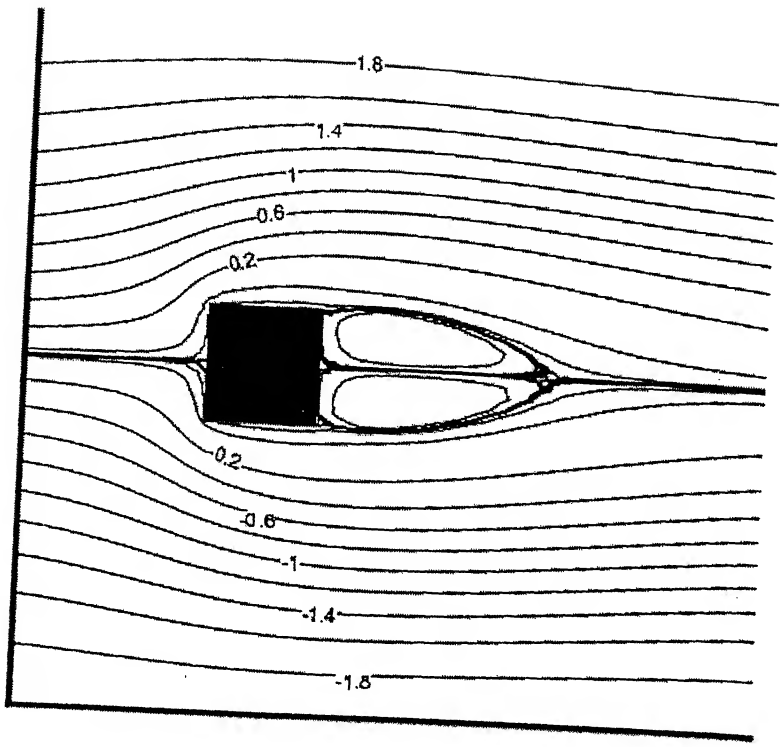

Figure 4.10

Streamlines pattern

Power Law Index: 1.4, Reynolds Number: 50.0,
Blockage Ratio: 1/6

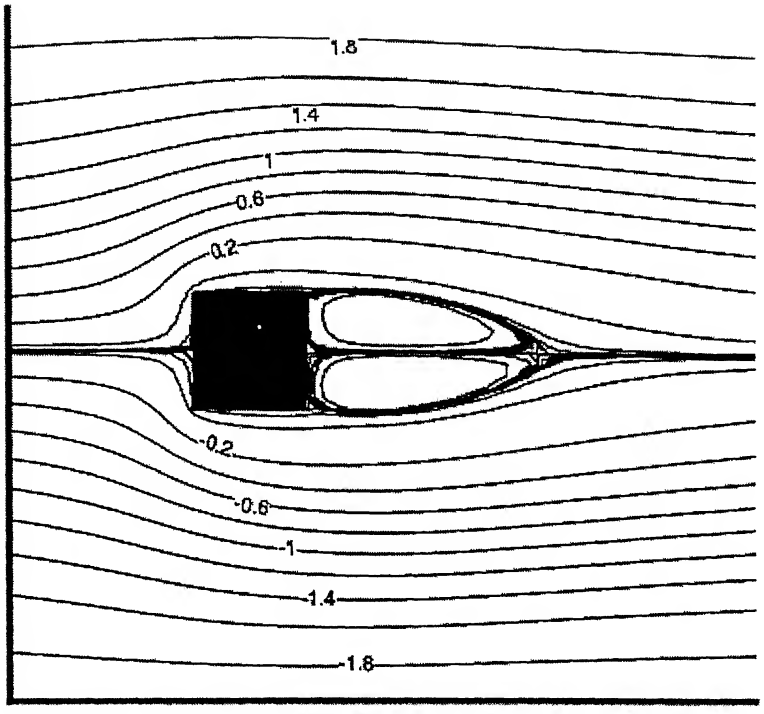

Figure 4.11

Streamlines pattern

Power Law Index: 1.6 , Reynolds Number: 50.0,
Blockage Ratio: 1/6

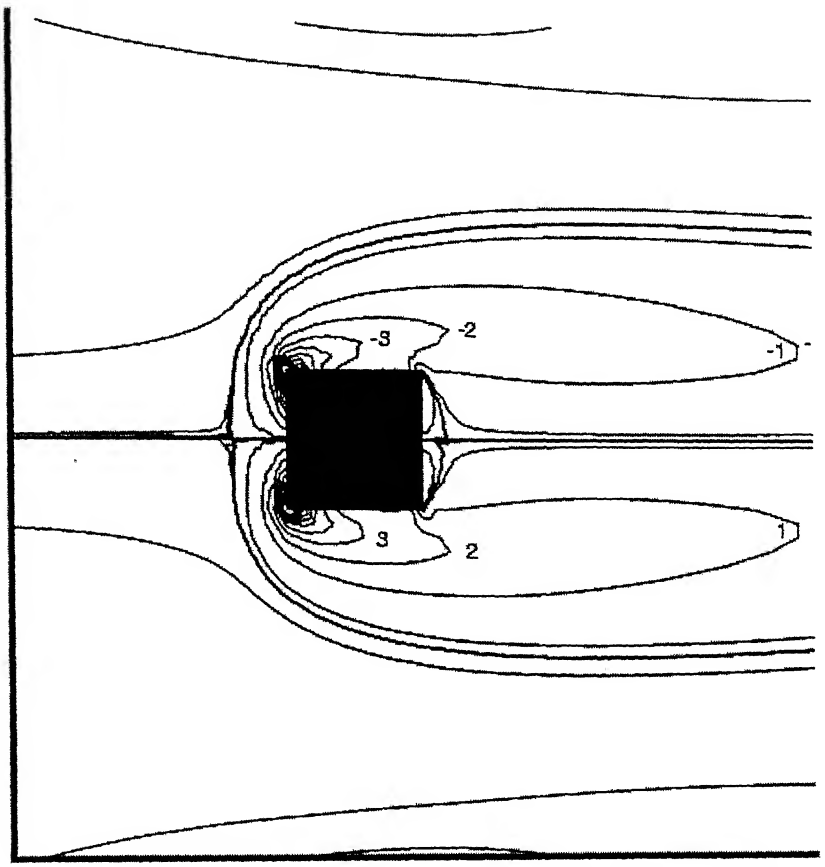

Figure 4.12

Iso-Vorticity Plot

Power Law Index=1.0
Blockage Ratio: 1/6, Reynolds Number: 50.0

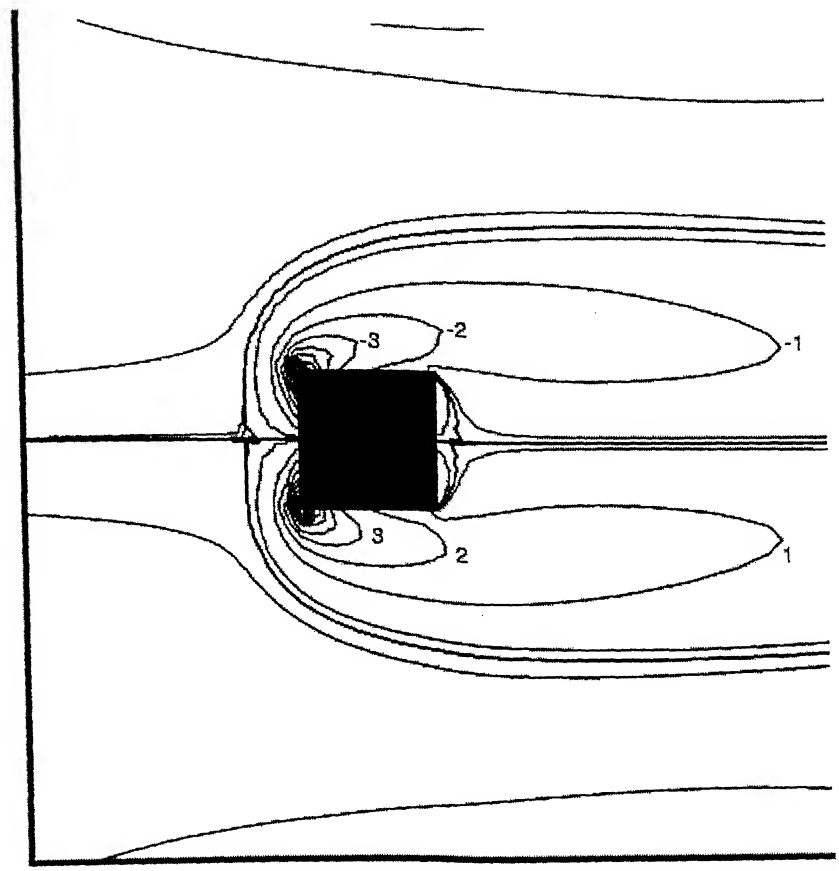

Figure 4.13

Iso-Vorticity Plot

Power Law Index=1.2
Blockage Ratio: 1/6, Reynolds Number: 50.0

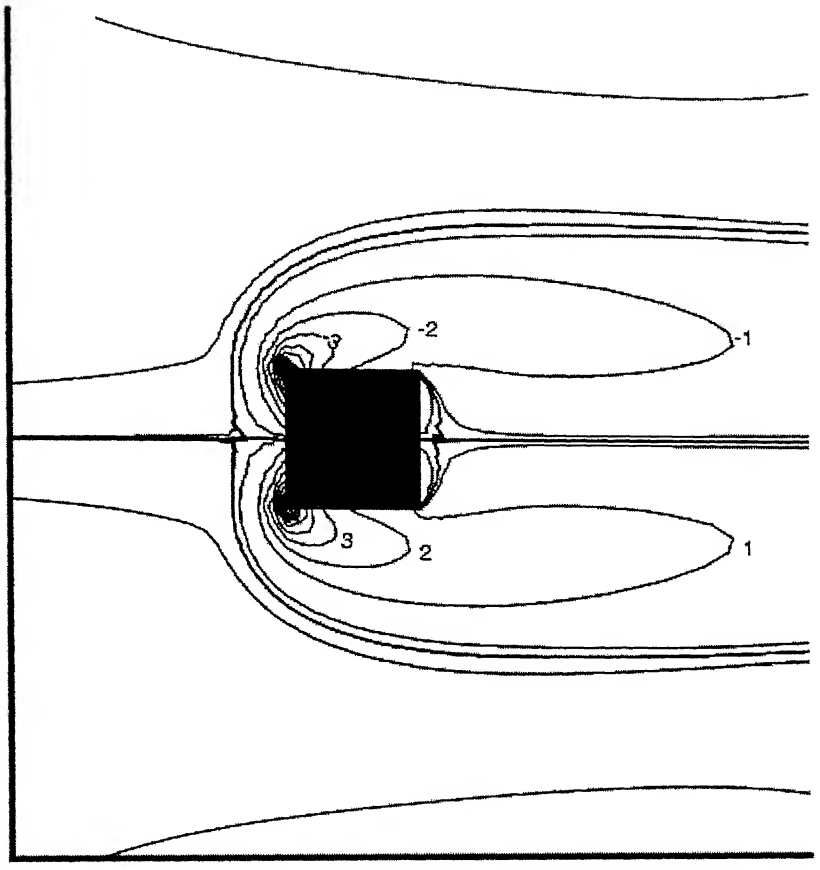

Figure 4.14

Iso-Vorticity Plot

Power Law Index=1.4
Blockage Ratio: 1/6, Reynolds Number: 50.0

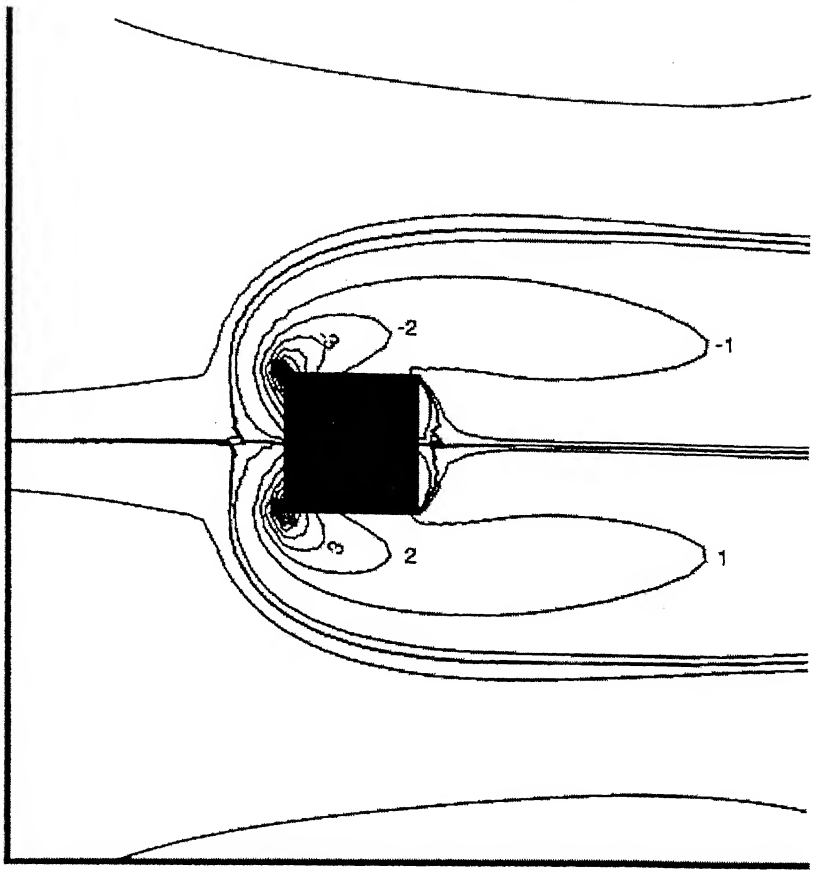

Figure 4.15

Iso-Vorticity Plot

Power Law Index=1.6
Blockage Ratio: 1/6, Reynolds Number: 50.0

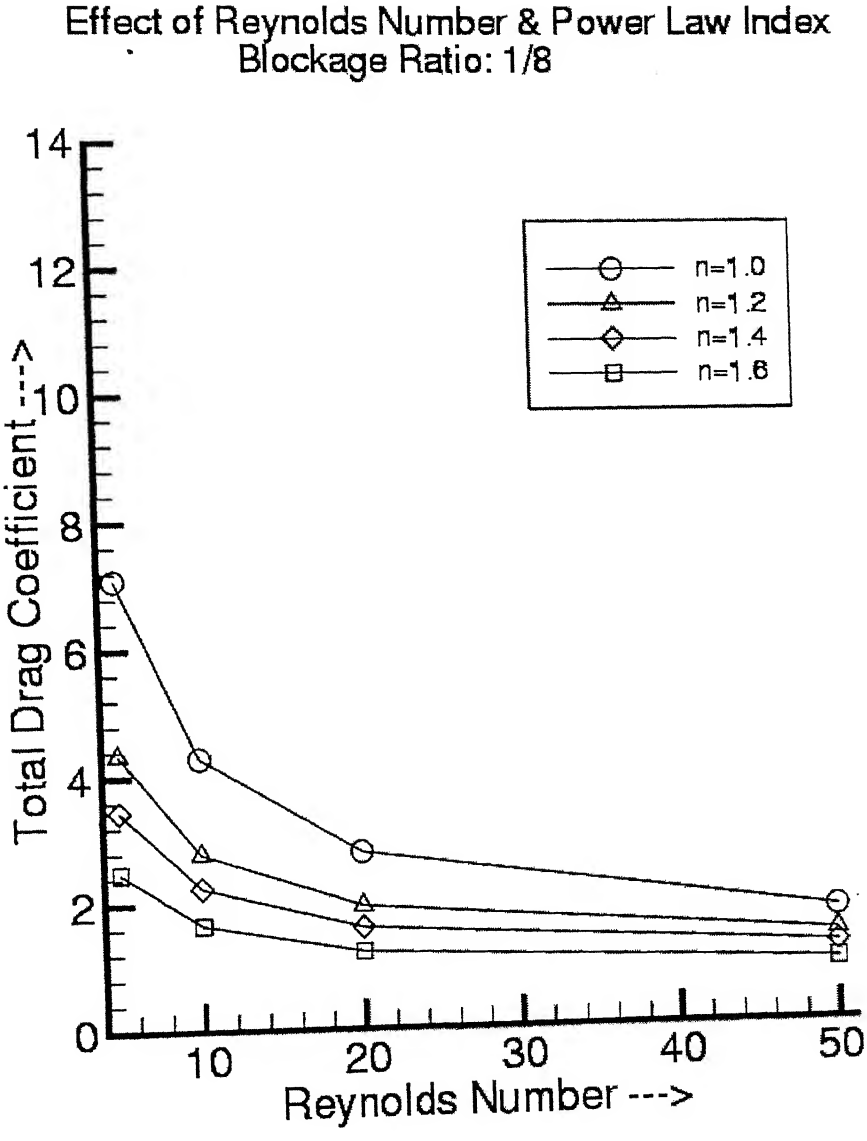
Effect of Reynolds Number & Power Law Index
Blockage Ratio: 1/8
Total Drag Coefficient --->
Reynolds Number --->
n=1.0
n=1.2
n=1.4
n=1.6
0
2
4
6
8
10
12
14
10
20
30
40
50

Figure 4.16

Effect of Reynolds Number & Power Law Index
Blockage Ratio: 1/6

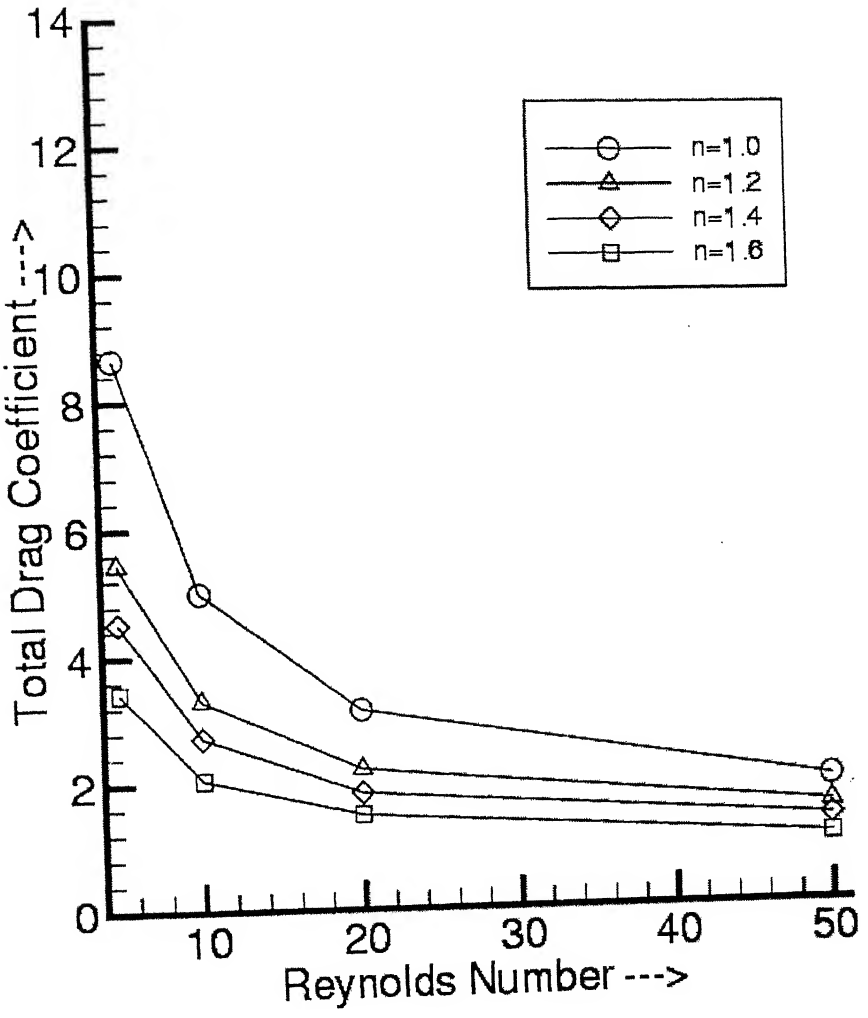

Figure 4.17

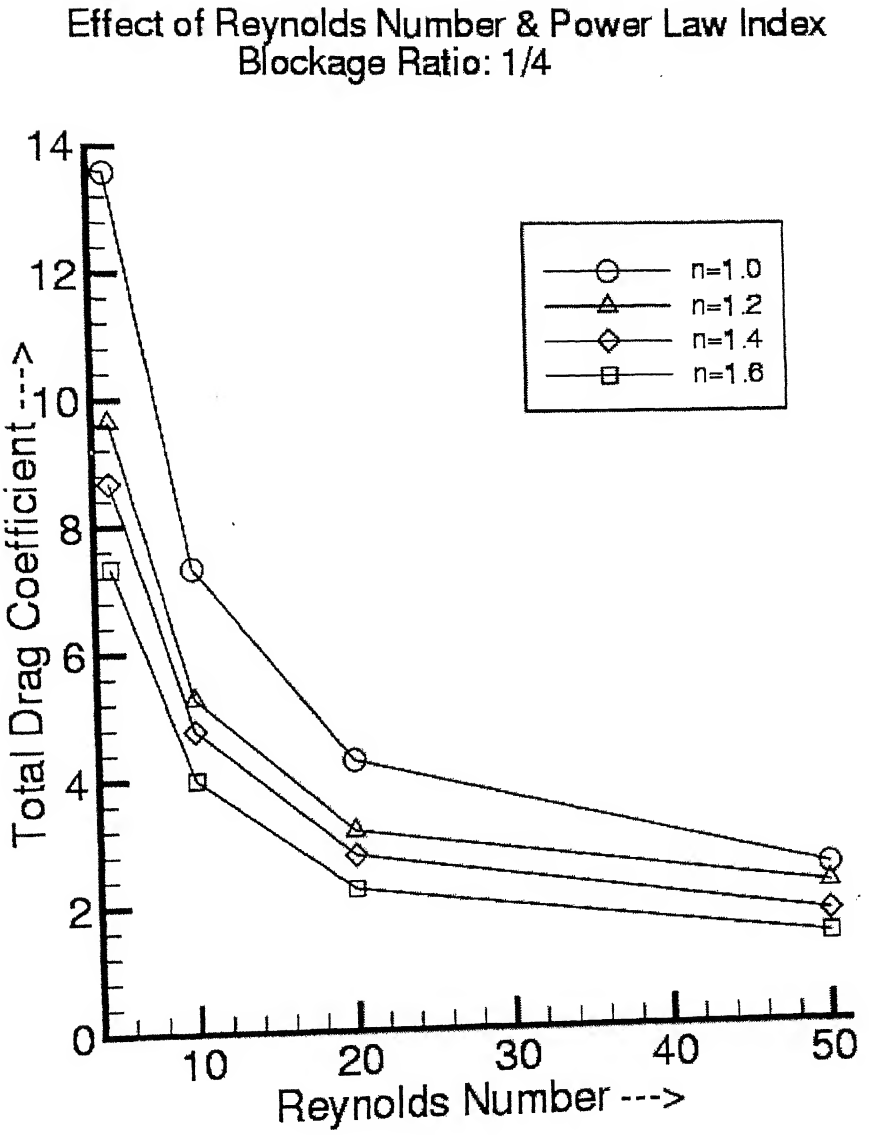
Effect of Reynolds Number & Power Law Index
Blockage Ratio: 1/4
Total Drag Coefficient --->
Reynolds Number --->
n=1.0
n=1.2
n=1.4
n=1.6
0
2
4
6
8
10
12
14
10
20
30
40
50

Figure 4.18

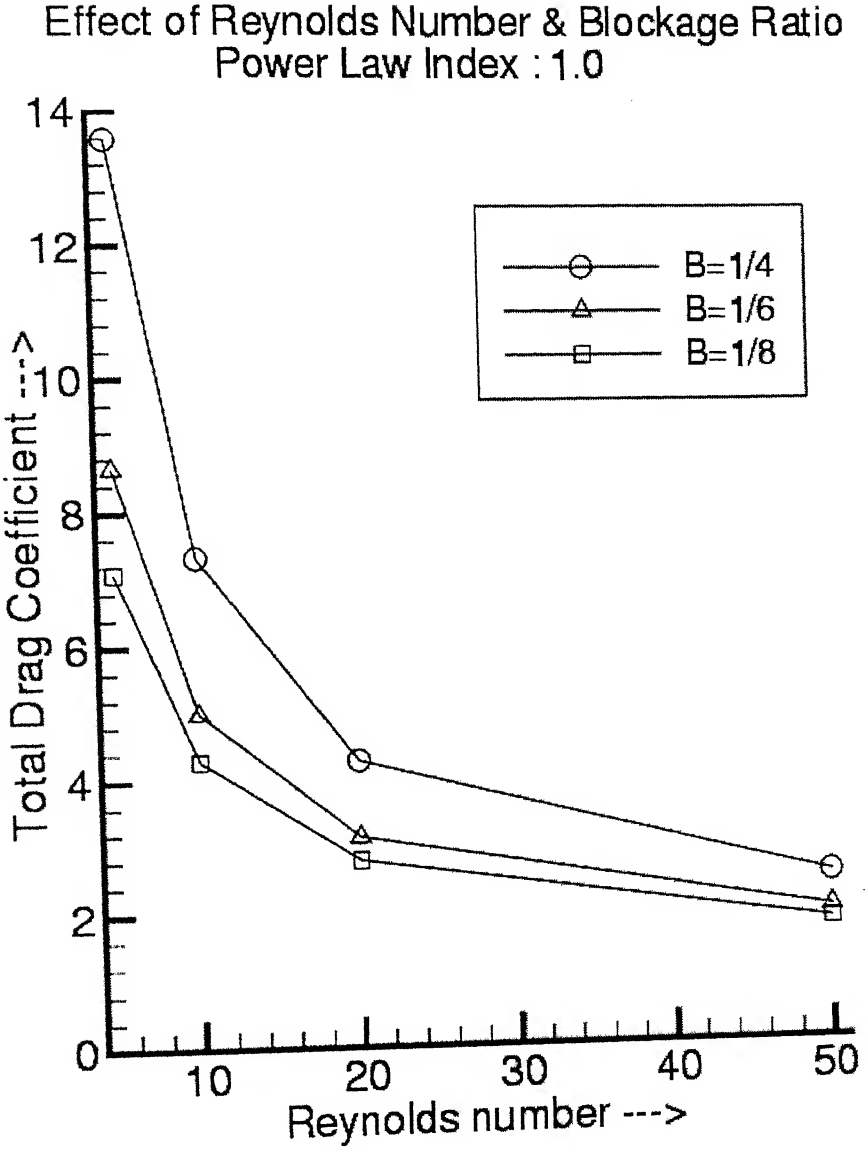

Figure 4.19

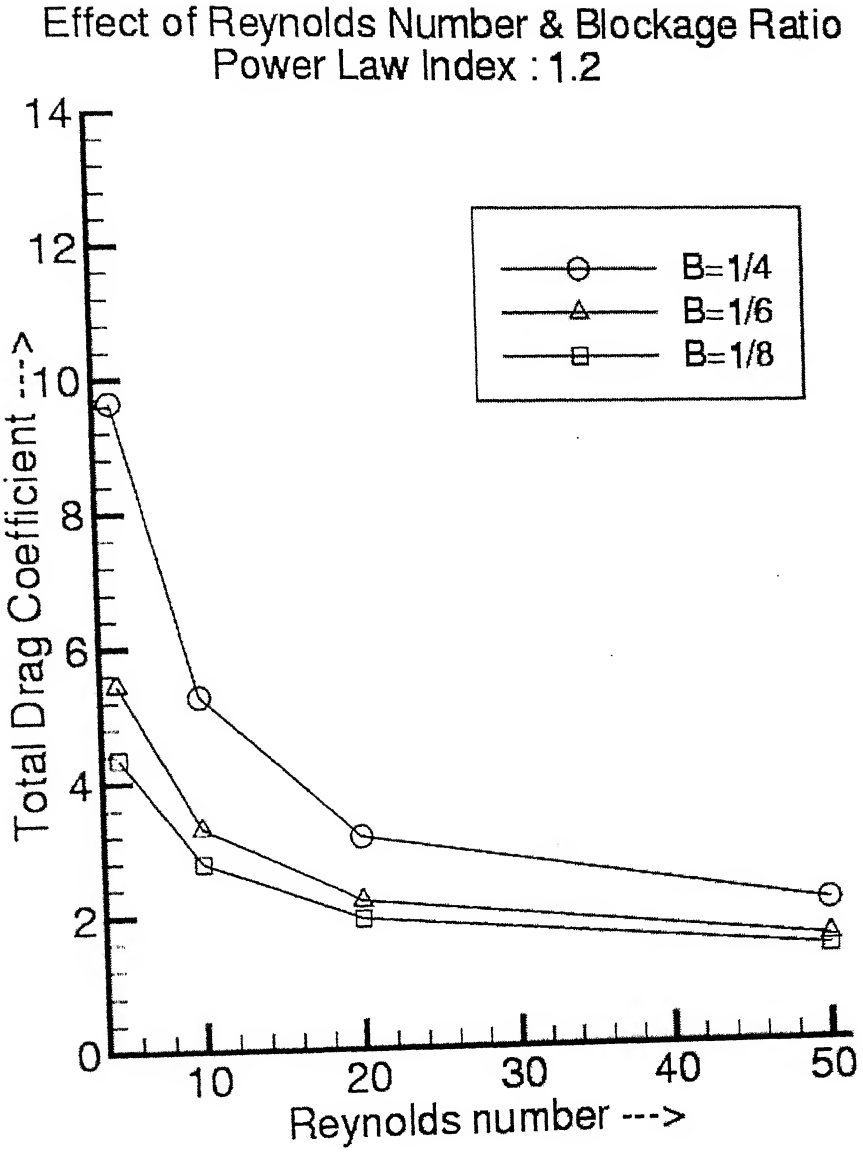
Effect of Reynolds Number & Blockage Ratio
Power Law Index : 1.2
Total Drag Coefficient --->
Reynolds number --->
B=1/4
B=1/6
B=1/8
0
2
4
6
8
10
12
14
10
20
30
40
50

Figure 4.20

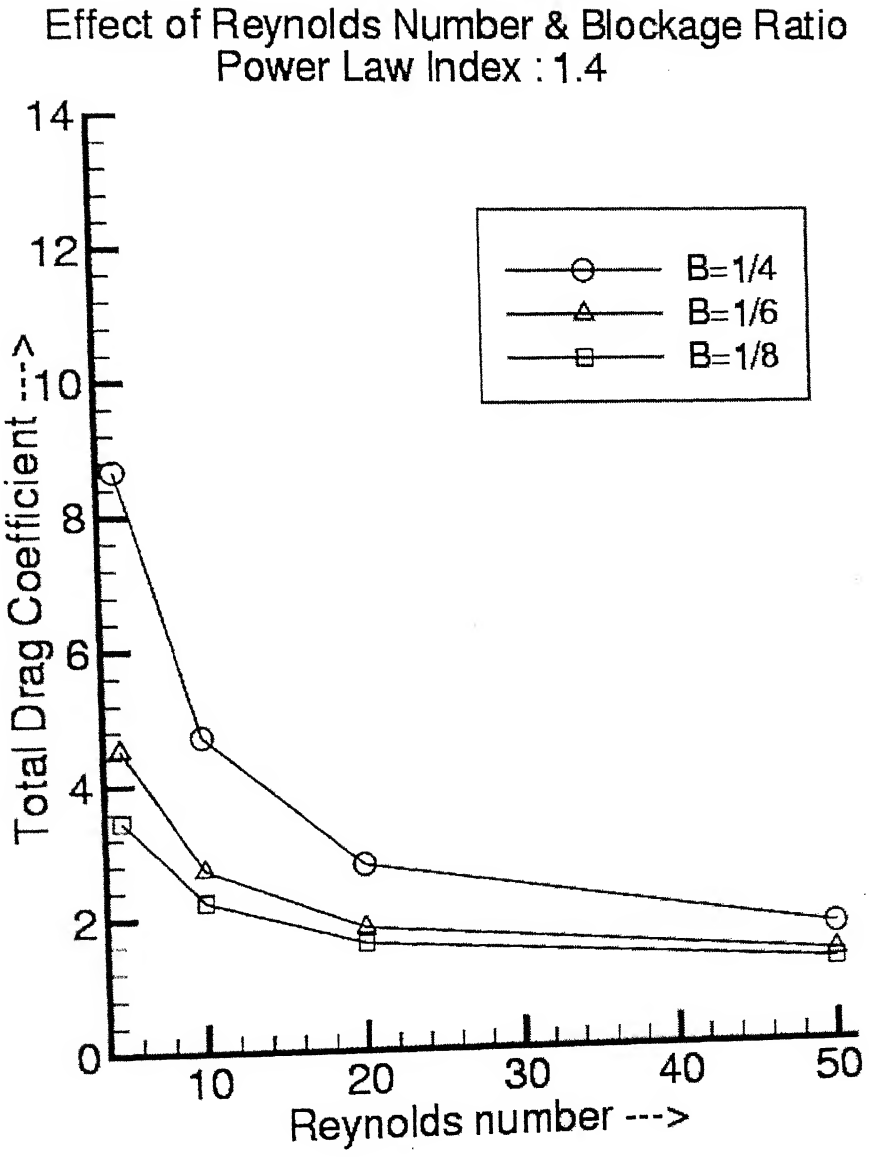
Effect of Reynolds Number & Blockage Ratio
Power Law Index : 1.4
Total Drag Coefficient --->
Reynolds number --->
B=1/4
B=1/6
B=1/8
0
2
4
6
8
10
12
14
10
20
30
40
50

Figure 4.21

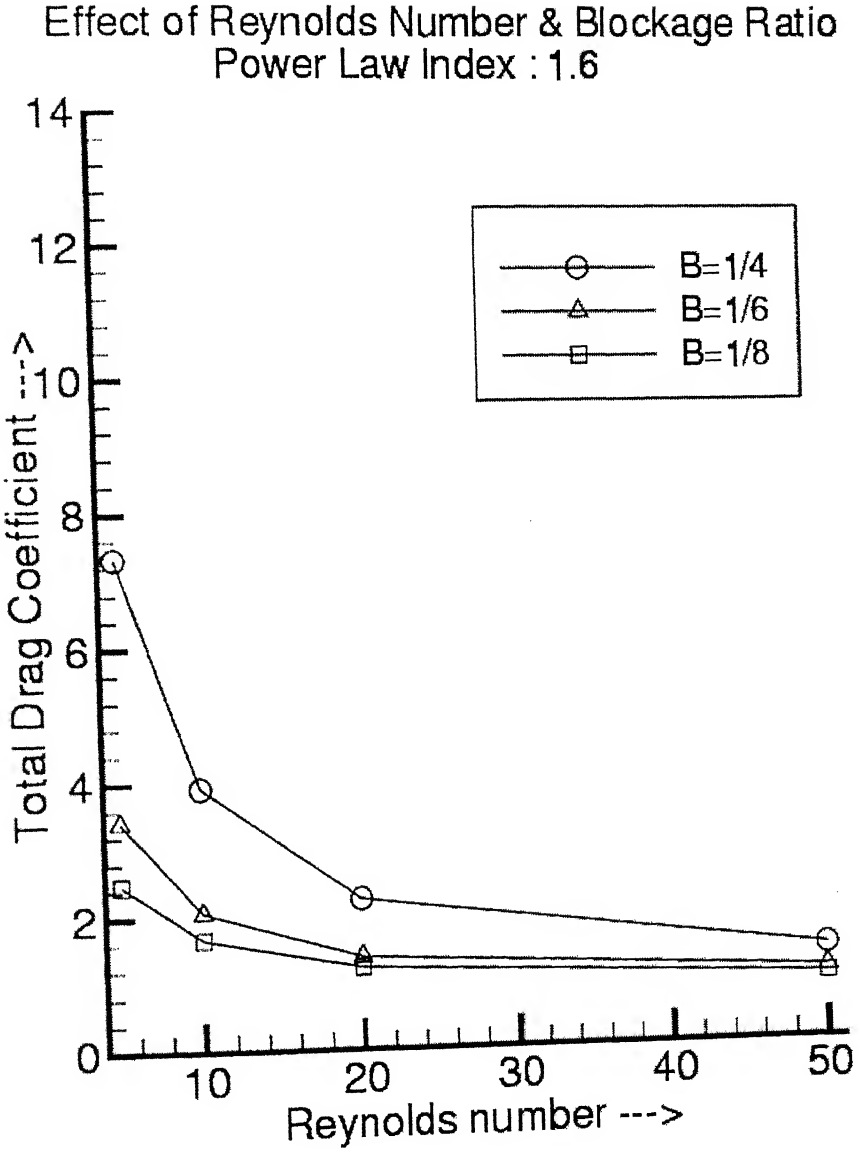
Effect of Reynolds Number & Blockage Ratio
Power Law Index : 1.6
B=1/4
B=1/6
B=1/8
Total Drag Coefficient --->
Reynolds number --->
0
2
4
6
8
10
12
14
10
20
30
40
50

Figure 4.22

Chapter 5

CONCLUSION AND SUGGESSIONS FOR FUTURE WORK

In the present work, Non-Newtonian (power law model) fluids flow past square cylinder placed in rectangular channel has been analyzed. The present problem has been solved with Stream function-Vorticity method. Problem has been solved on the uniform grid spacing. In particular, the detailed kinematics of the flow in terms of the values of stream function and vorticity has been obtained. Further, the values of stream function and vorticity were used to calculate pseudo-pressure field. Finally velocity field and pressure field were used to calculate the individual coefficient of drags and total coefficient of drag. The present study covers the low Reynolds number range $(5.0 \leq \mathrm{Re} \leq 50.0)$. The shear thickening effect $(1.0 \leq n \leq 1.6)$ and blockage ratio $(1/8,1/6,1/4)$ has been studied. The following points can be concluded from the present work

1. The flow remains steady below 50.0 Reynolds number for all values of power law index. In the wake of the cylinder, a steady axi-symmetric recirculation region is observed. The length of this recirculation region increases with increase in Reynolds number.

2. At a constant value of power law index and blockage ratio, the viscous drag coefficient, form drag coefficient and total drag coefficient decrease with increase in Reynolds number.

3. At a constant value of Reynolds number and blockage ratio, the length of recirculation region increases with increase in power law index. This can be explained by analyzing the figure 5.1. It is clear from the figure that as the power law index increases (implying high viscosity near the cylinder surface) the stream function contour line of the same value ($\psi = 0.1$) goes away from the cylinder. So this creates long recirculation region in the wake. The total coefficient of drag decreases with increase in power law index.

4. At a constant value of Reynolds number and power law index, the viscous drag coefficient, form drag coefficient and total drag coefficient increase with increase in blockage ratio.

Suggestion for future work:

The work reported herein should be extended to:

1. elucidate the role of shear thinning on drag as well as on the streamlines and vorticity plots.
2. calculate the heat transfer characteristics such as Nusselt number for shear thickening and shear thinning fluids.

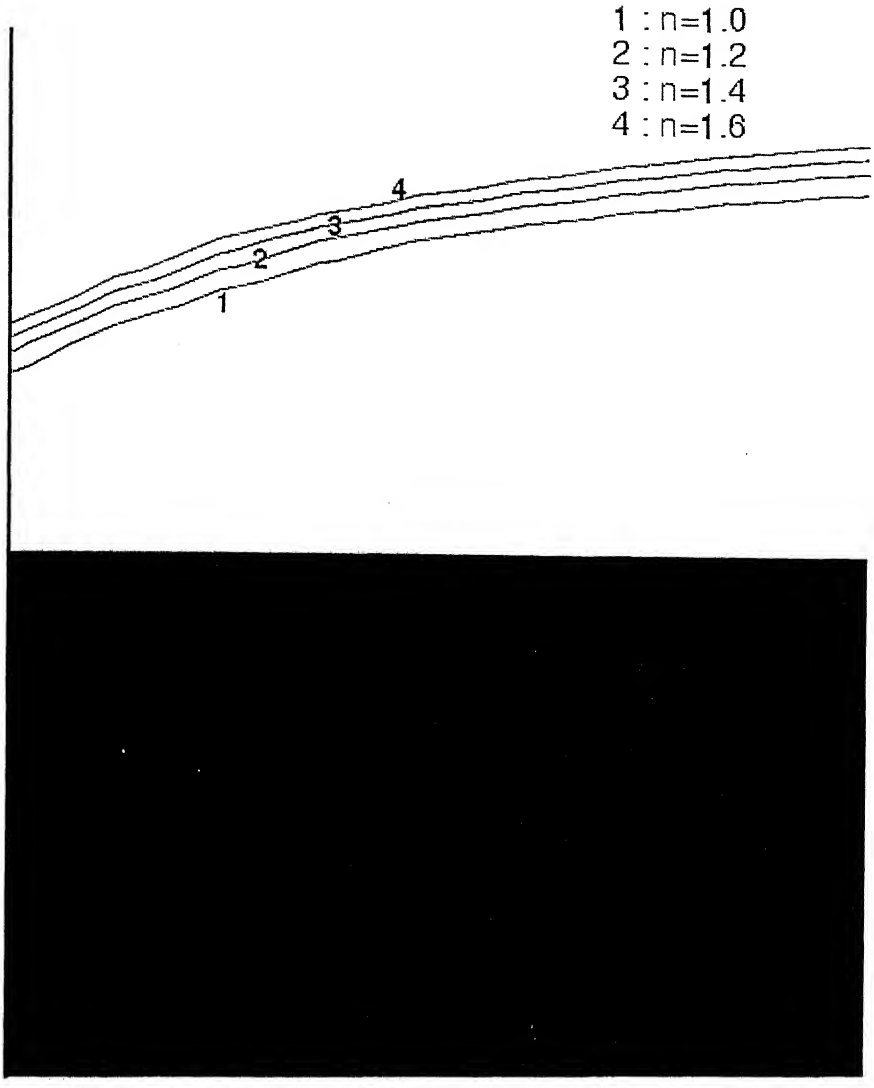

Stream lines for different value of Power Law Index for same value of stream function (ψ=0.1)
Re=50.0 , B=1/6

Figure 5.1

[8] Saha, A.K., Muralidhar, K., Biswas, G., 2000. *Vortex structure and kinetic energy budget in two-dimensional flow past a square cylinder.* Computers & Fluids 29, 669-694.

[9] Breuer, M., Bernsdorf, J., Zeiser, T., Durst, F., 2000. *Accurate computations of the laminar flow past a square cylinder based on two different methods: lattice-Boltzmann and finite-volume.* Int. J. Heat and Fluid Flow 21, 186-196.

[10] Bird, R.B., Stewart, W.E., Lightfoot E.N., 2001. *Transport Phenomena*, 2nd edition John Wiley, New York.